Journal of Organometallic Chemistry 1014 (2024) 123185

Contents lists available at ScienceDirect

Journal of Organometallic Chemistry

journal homepage: www.elsevier.com/locate/jorganchem

# The influence of phosphine ligands on the redox properties of 1,4-divinylanthrylene-bridged diruthenium complexes and a derived macrocyclic analog

Franciska S. Gogesch [a], Jonas Rendler [a], Michael Linseis [a], Laura Senft [b], Ivana Ivanović-Burmazović [b], Rainer F. Winter [a,*]

[a] Fachbereich Chemie, Universität Konstanz, Universitätsstraße 10, 78457 Konstanz, Germany
[b] Department Chemie, Ludwig-Maximilians-Universität München, Butenandstraße 5-13, Haus D, 81377 München, Germany

ARTICLE INFO

*Keywords:*
Ruthenium alkenyl complexes
Mixed-valent compounds
(spectro)electrochemistry
Phosphine ligands
Anthrylene
Metallamacrocycle

ABSTRACT

We report on a series of dinuclear 1,4-divinylanthrylene-bridged diruthenium complexes **1A-Ru-PR$_3$** with different phosphine ligands (P$^i$Pr$_3$, P$^i$Pr$_2$Me, PPh$_3$, and PMe$_3$) and with coordination numbers of five or six. All compounds were characterized by NMR spectroscopy, high resolution ESI-MS and, in the case of **1A-Ru-P$^i$Pr$_3$** and **1A-Ru-PMe$_3$**, single crystal X-ray diffraction. Cyclic voltammetry measurements reveal that the PR$_3$ ligands, besides tuning the redox potentials, exert a strong influence on the stability of their one- and two-electron oxidized forms. Information on the charge- and spin-density distribution was obtained by IR, UV/Vis/NIR and EPR spectroscopy. Our results indicate full charge and spin delocalization in **1A-Ru-P$^i$Pr$_3^{\bullet+}$**, **1A-Ru-PMe$_3^{\bullet+}$** and macrocyclic, isophthalate-bridged **2A-Ru-P$^i$Pr$_2$Me$^{\bullet\bullet 2+}$**, whereas **1A-Ru-P$^i$Pr$_2$Me$^{\bullet+}$** constitutes a peculiar case, where valence-delocalized and valence-localized structures seem to coexist.

## 1. Introduction

Bis(alkenyl)arylene-bridged diruthenium complexes of the general type [{Ru}$_2$($\mu$-CH=CH−Aryl−CH=CH)] ({Ru} = {(PR$_3$)$_2$(L)(CO)Ru; *L* = PR$_3$ with *R* = $^i$Pr [1–6], Ph [7–10], Me [11–21], Et or a vacant coordination site [22], or (L)(X) = bidentate monoanionic carboxylate [23,24] or $\beta$-ketoenolate ligand [25–27]) exhibit several remarkable properties such as: i) Two consecutive one-electron oxidations at low potentials. Additional oxidations may ensue, if the bridging ligand is redox-active by itself. ii) (Poly)electrochromic behavior with strong absorption of the oxidized states in the visible (Vis) and the near infrared (NIR) as a result of large or even dominant bridge contributions to the individual redox processes. iii) The Ru(CO) band(s) as sensitive, local probes for the electron density at the ruthenium ions and its alteration during a redox process. Any loss of charge density from the metal ions will cause a blue-shift of the CO stretching vibration(s), whose magnitude scales with metal contribution to the respective "redox orbital". In dinuclear complexes, the pattern of Ru(CO) bands is also indicative of a symmetric versus asymmetric charge distribution within such a conjugated metal-organic π-system. iv) Resolved hyperfine splittings (hfs) to the $^{31}$P and $^{99/101}$Ru nuclei in EPR spectra of the one-electron oxidized, mixed-valent (MV) radical cations reveal, whether the unpaired spin density is evenly or asymmetrically distributed over the two ruthenium sites.

Alkenyl complexes [(PPh$_3$)$_3$Cl(CO)Ru-CH=CHR] generally engage in dynamic equilibria between red- to purple-colored five- and yellow six-coordinated forms with either two or three PPh$_3$ ligands attached to the ruthenium ion [8,10]. The ensuing non-ideal electrochemical behavior and their often poor solubilities are obstacles in explorations of their oxidized forms. They are hence often primarily used as intermediates for better soluble, stable six-coordinated complexes with three PMe$_3$ or PEt$_3$ ligands [11,15,22,28–31], which have been the subject of extensive studies [11–14,21,32].

While sterically less demanding phosphine ligands allow for coordinative saturation of the ruthenium ions, the bulkier, strongly electron-donating P$^i$Pr$_3$, PCy$_3$ (Cy = cyclohexyl) or P$^i$Pr$_2$R (R = Ph, Me) ligands form only diphosphine complexes of coordination number five [33–41]. In these cases, the metal ions adopt a slightly distorted square pyramidal geometry with the alkenyl ligand in the apical position. Despite their 16 valence electron (VE) count, the ruthenium ions in these complexes are

* Corresponding author.
*E-mail address:* Rainer.Winter@uni-konstanz.de (R.F. Winter).

https://doi.org/10.1016/j.jorganchem.2024.123185
Received 12 March 2024; Received in revised form 10 May 2024; Accepted 14 May 2024
Available online 15 May 2024

even more electron-rich than their 18 VE $PMe_3$ congeners, as indicated by the lower energies of their CO stretches. Moreover, they oxidize at lower potential and provide radical cations of superior chemical stability [1,12,42,43]. Bulky phosphine ligands however cover a large part of π-conjugated linker, thereby inhibiting intermolecular interactions, e.g. with electron acceptors [23,44–47]. Whereas the effects of attaching electron-donating or -withdrawing substituents to the aryl or arylene entities of mono- or dinuclear ruthenium complexes of this type are broadly documented [11,12,29,42,43,48], systematic studies devoted to the impact of the $PR_3$ coligands are comparatively scarce [10,36,41,49]. The present work utilizes the common template of a 1,4-divinylanthrylene-bridged diruthenium complex in conjunction with $P^iPr_3$, $P^iPr_2Me$, $PPh_3$, and $PMe_3$ ligands for this purpose.

## 2. Experimental

### 2.1. Methods and materials

All manipulations were performed under an atmosphere of purified nitrogen with dry, distilled, and nitrogen-saturated solvents. All reagents were purchased from commercial vendors and used without further purification. $^1$H NMR (800 MHz), $^{31}$P NMR (324 MHz), and $^{13}$C NMR (202 MHz) spectra were measured on a Bruker Avance Neo 800 spectrometer, $^1$H NMR (600 MHz) and $^{13}$C NMR (151 MHz) spectra were measured on a Bruker Avance III 600 spectrometer, and $^{31}$P NMR (162 MHz) spectra were measured on a Bruker Avance III 400 spectrometer. The precursor **LA-H** [50] and the hydride complexes [H-{Ru}] with $P^iPr_3$ [51], $P^iPr_2Me$ [40], and $PPh_3$ [52] were prepared according to published procedures.

### 2.2. Synthesis and characterization

#### 2.2.1. General synthetic procedure

1,4-Diethynylanthracene (1.00 eq.) was dissolved in $CH_2Cl_2$ (20 mL) and added dropwise to a solution of the respective [H-{Ru}] complex (2.10 equiv.) in $CH_2Cl_2$ (20 mL). The reaction mixture was stirred for 1 h at r.t. The solvent was removed under reduced pressure and the residue was washed with $^n$hexane for **1A-Ru-P$^i$Pr$_3$** and **1A-Ru-P$^i$Pr$_2$Me**, or with $Et_2O$ for **1A-Ru-PPh$_3$** to yield the respective bis(alkenyl)ruthenium complex.

#### 2.2.2. 1A-Ru-P$^i$Pr$_3$

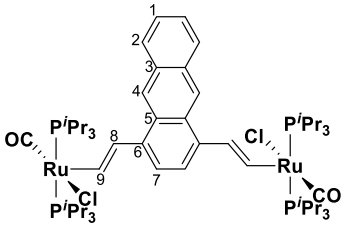


**Yield:** 93%

$^1$H NMR (800 MHz, $C_6D_6$): δ [ppm] = 9.13 (s, 2H, $H_{(4)}$), 9.03 (d, $^3J_{HH}$ = 12.8 Hz, 2H, $H_{(9)}$), 7.93 (dd, $^3J_{HH}$ = 6.4 Hz, $^4J_{HH}$ = 3.2 Hz, 2H, $H_{(2)}$), 7.73 (s, 2H, $H_{(7)}$), 7.40 (dt, $^3J_{HH}$ = 12.8 Hz, $^4J_{HP}$ = 2.3 Hz, 2H, $H_{(8)}$), 7.25 (dd, $^3J_{HH}$ = 6.4 Hz, $^4J_{HH}$ = 3.2 Hz, 2H, $H_{(1)}$), 2.70 – 2.63 (m, 12H, PC*H*(CH$_3$)$_2$), 1.23 – 1.17 (m, 72H, PCH(C*H*$_3$)$_2$). $^{31}$P{$^1$H} NMR (324 MHz, $C_6D_6$): δ [ppm] = 37.74 (s). $^{13}$C{$^1$H} NMR (201 MHz, $C_6D_6$): δ [ppm] = 204.1 (t, $^2J_{CP}$ = 13.2 Hz, *C*O), 152.9 (t, $^2J_{CP}$ = 11.1 Hz, $C_{(9)}$), 134.0 (s, $C_{(6)}$), 132.2 (s, $C_{(3)}$), 131.6 (s, $C_{(8)}$), 130.1 (s, $C_{(5)}$), 128.9 (s, $C_{(2)}$), 125.2 (s, $C_{(1)}$), 123.3 (s, $C_{(4)}$), 122.5 (s, $C_{(7)}$), 24.7 (vt, $^{1,3}J_{CP}$ = 9.8 Hz, P*C*H(CH$_3$)$_2$), 20.1 (s, PCH(*C*H$_3$)$_2$), 19.9 (s, PCH(*C*H$_3$)$_2$). HRMS (ESI) ($CH_2Cl_2$): *m/z* calcd. for $Ru_2P_4Cl_2C_{56}H_{96}O_2^+$ ($M^+$) 1198.3837, found 1198.3820.

#### 2.2.3. 1A-Ru-P$^i$Pr$_2$Me

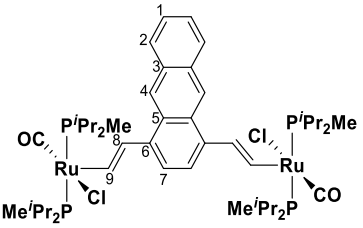


**Yield:** 79 %

$^1$H NMR (800 MHz, $C_6D_6$): δ [ppm] = 9.14 (s, 2H, $H_{(4)}$), 8.76 (d, $^3J_{HH}$ = 12.4 Hz, 2H, $H_{(9)}$), 7.91 (dd, $^3J_{HH}$ = 6.4 Hz, $^4J_{HH}$ = 3.2 Hz, 2H, $H_{(2)}$), 7.62 (s, 2H, $H_{(7)}$), 7.27 (d, $^3J_{HH}$ = 12.4 Hz, 2H, $H_{(8)}$), 7.25 (dd, $^3J_{HH}$ = 6.4 Hz, $^4J_{HH}$ = 3.2 Hz, 2H, $H_{(1)}$), 2.80 – 2.75 (m, 4H, PC*H*(CH$_3$)$_2$), 1.87 (s, 4H, PC*H*(CH$_3$)$_2$), 1.21 (vt, $^{1,3}J_{HP}$ = 3.1 Hz, 12H, PCH$_3$), 1.17 – 1.10 (m, 36H, PCH(C*H*$_3$)$_2$), 0.83 – 0.77 (m, 12H, PCH(C*H*$_3$)$_2$). $^{31}$P {$^1$H} NMR (162 MHz, $C_6D_6$): δ [ppm] = 29.46 (s). $^{13}$C {$^1$H} NMR (202 MHz, $C_6D_6$): δ [ppm] = 203.5 (t, $^2J_{CP}$ = 12.7 Hz, *C*O), 153.0 (t, $^2J_{CP}$ = 8.5 Hz, $C_{(9)}$), 134.3 (s, $C_{(6)}$), 131.7 (s, $C_{(3)}$), 130.7 (s, $C_{(8)}$), 130.2 (s, $C_{(5)}$), 128.9 (s, $C_{(2)}$) 125.3 (s, $C_{(1)}$), 123.3 (s, $C_{(4)}$), 122.4 (s, $C_{(7)}$), 26.8 (vt, $^{1,3}J_{CP}$ = 12.1 Hz, P*C*H(CH$_3$)$_2$), 22.3 (vt, $^{1,3}J_{CP}$ = 12.1 Hz, P*C*H(CH$_3$)$_2$), 19.6 (s, PCH(*C*H$_3$)$_2$), 19.3 (s, PCH(*C*H$_3$)$_2$), 18.6 (s, PCH(*C*H$_3$)$_2$), 17.0 (s, PCH(*C*H$_3$)$_2$), 3.3 (vt, $^{1,3}J_{CP}$ = 13.3 Hz, P*C*H$_3$). HRMS (ESI) ($CH_2Cl_2$): *m/z* calcd. for $Ru_2P_4Cl_2C_{48}H_{80}O_2^+$ ($M^+$) 1086.2582, found 1086.2574.

#### 2.2.4. 1A-Ru-PPh$_3$

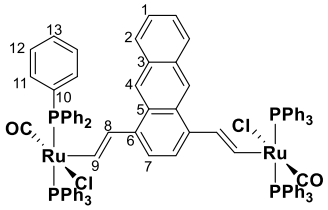


**Yield:** 90 %

$^1$H NMR (600 MHz, $CD_2Cl_2$): δ [ppm] = 8.51 (dt, $^3J_{HH}$ = 12.6 Hz, $^3J_{HP}$ = 2.2 Hz, 2H, $H_{(9)}$), 8.15 (s, 2H, $H_{(4)}$), 7.88 (dd, 2H, $^3J_{HH}$ = 6.5 Hz, $^4J_{HH}$ = 3.0 Hz $H_{(2)}$), 7.63 – 7.59 (m, 24H, $H_{(12)}$), 7.49 (t, $^3J_{HH}$ = 7.4 Hz, 12H, $H_{(13)}$), 7.45 (dd, $^3J_{HH}$ = 6.5 Hz, $^4J_{HH}$ = 3.6 Hz, 2H, $H_{(1)}$), 7.41 (t, $^3J_{HH}$ = 7.4 Hz, 24H, $H_{(11)}$), 6.61 (dt, $^3J_{HH}$ = 12.6 Hz, $^4J_{HH}$ = 2.1 Hz, 2H, $H_{(8)}$), 6.58 (s, 2H, $H_{(7)}$). $^{31}$P {$^1$H} NMR (162 MHz, $C_6D_6$): δ [ppm] = 31.39 (s). $^{13}$C {$^1$H} NMR could not be measured due to low solubility. HRMS (ESI) ($CH_2Cl_2$): *m/z* calcd. for $Ru_2P_3Cl_3C_{74}H_{57}O_2$ ($M^+$- $PPh_3$ + Cl), 1379.0737, found 1379.1063. Anal. Calcd. for $Ru_2P_4Cl_2C_{92}H_{72}O_2^+$: C 68.78%, H 4.52%; found C 68.53%, H 4.70%.

#### 2.2.5. 1A-Ru-PMe$_3$

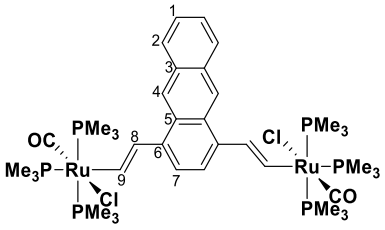


**1A-Ru-PPh$_3$** (78.0 mg, 0.05 mmol, 1.00 eq.) was dissolved in $CH_2Cl_2$ (20 mL) and $PMe_3$ (36.9 mg, 0.05 mL, 10.00 eq.) was added. The reaction mixture was stirred for 20 h at r.t. The reaction mixture was concentrated under reduced pressure and $^n$hexane (20 mL) was added. The formed precipitate was collected and was washed with $^n$hexane (3 × 20 mL). The residue was dissolved in $Et_2O$ (20 mL) and insoluble impurities were removed. The solvent was removed under reduced pressure to give **1A-Ru-PMe$_3$** in 83% yield (41.2 mg, 0.04 mmol).

$^1$H NMR (600 MHz, $CD_2Cl_2$): δ [ppm] = 8.87 (s, 2H, $H_{(4)}$), 8.19 (ddt, $^3J_{HH}$ = 17.5 Hz, $^3J_{HP}$ = 8.4 Hz, 3.4 Hz, 2H, $H_{(9)}$), 8.00 (dd, $^3J_{HH}$ = 6.5 Hz, $^4J_{HH}$ = 3.2 Hz, 2H, $H_{(2)}$), 7.56 (s, 2H, $H_{(7)}$), 7.49 (ddt, $^3J_{HH}$ = 17.5 Hz,

$^{4}J_{HP}$ = 6.4 Hz, 2.5 Hz, 2H, $H_{(8)}$), 7.41 (dd, $^{3}J_{HH}$ = 6.5 Hz, $^{4}J_{HH}$ = 3.2 Hz, 2H, $H_{(1)}$), 1.50 (d, $^{2}J_{HP}$ = 6.8 Hz, 18H, P(C$\underline{H}_3$)$_3$), 1.45 (vt, $^{2,4}J_{HP}$ = 3.5 Hz, 36H, P(C$\underline{H}_3$)$_3$). $^{31}$P {$^{1}$H} NMR (162 MHz, $CD_2Cl_2$): δ [ppm] = −7.01 (d, $^{2}J_{PP}$ = 22.9 Hz), −19.28 (t, $^{2}J_{PP}$ = 22.9 Hz). $^{13}$C {$^{1}$H} NMR (151 MHz, $CD_2Cl_2$): δ [ppm] = 203.1 (dt, $^{2}J_{CP}$ = 13.2 Hz, $^{2}J_{CP}$ = 11.4 Hz, $\underline{C}$O), 169.1 (d, $^{2}J_{CP}$ = 76.9 Hz, $C_{(9)}$), 136.2 (dt, $^{4}J_{CP}$ = 7.4 Hz, $^{4}J_{CP}$ = 2.5 Hz, $C_{(6)}$), 131.5 (t, $^{3}J_{CP}$ = 4.7 Hz, $C_{(8)}$), 131.0 (s, $C_{(3)}$), 130.2 (s, $C_{(5)}$), 128.7 (s, $C_{(2)}$), 125.0 (s, $C_{(1)}$), 122.8 (s, $C_{(4)}$), 121.7 (s, $C_{(7)}$), 20.2 (dt, $^{1}J_{CP}$ = 21.0 Hz, $^{3}J_{CP}$ = 1.7 Hz, P($\underline{C}$H$_3$)$_3$), 16.9 (vtd, $^{1,3}J_{CP}$ = 15.3 Hz, $^{3}J_{CP}$ = 2.2 Hz, P($\underline{C}$H$_3$)$_3$). HRMS (ESI) ($CH_2Cl_2$): *m/z* calcd. for $Ru_2P_6Cl_2C_{38}H_{66}O_2^+$ ($M^+$) 1014.0958, found 1014.0947.

### 2.2.6. 2A-Ru-P$^i$Pr$_2$Me

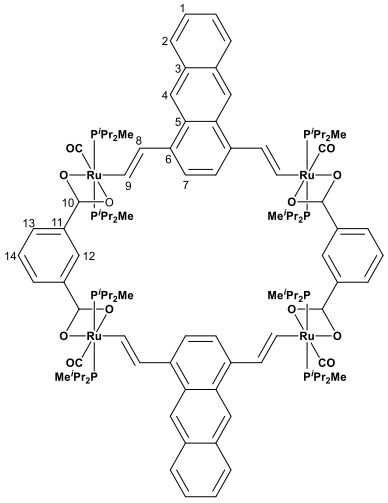


Isophthalic acid (12.1 mg, 0.07 mmol, 1.00 eq.) and $K_2CO_3$ (20.1 mg, 0.15 mmol, 2.00 eq.) were dissolved in methanol (20 mL) and added dropwise to a solution of **1A-Ru-P$^i$Pr$_2$Me** (78.8 mg, 0.07 mmol, 1.00 eq.) in $CH_2Cl_2$ (20 mL). The reaction mixture was stirred for 16 h at r.t. During this time, copious amounts of insoluble material were formed. The reaction mixture was concentrated under reduced pressure and the formed precipitate was collected. The residue was dissolved in $CH_2Cl_2$ (20 mL) and insoluble salts were removed. The solvent was removed under reduced pressure and the obtained solid was washed with $^n$hexane (2 × 20 mL) and methanol (20 mL) to obtain **2A-Ru-P$^i$Pr$_2$Me** in 10% yield (17.3 mg, 0.01 mmol).

$^{1}$H NMR (600 MHz, $C_6D_6$): δ [ppm] = 9.44 (s, 4H, $H_{(4)}$), 9.30 (dt, $^{3}J_{HH}$ = 15.0 Hz, $^{3}J_{HP}$ = 1.8 Hz, 4H, $H_{(9)}$), 9.28 (t, $^{4}J_{HH}$ = 1.6 Hz, 2H, $H_{(12)}$), 8.39 (dd, $^{3}J_{HH}$ = 7.6 Hz, $^{4}J_{HH}$ = 1.6 Hz, 4H, $H_{(13)}$), 8.17 (s, 4H, $H_{(7)}$), 7.99 (dd, $^{3}J_{HH}$ = 6.4 Hz, $^{4}J_{HH}$ = 3.2 Hz, 4H, $H_{(2)}$), 7.73 (dt, $^{3}J_{HH}$ = 15.0 Hz, $^{4}J_{HP}$ = 2.3 Hz, 4H, $H_{(8)}$), 7.24 (dt, $^{3}J_{HH}$ = 6.4 Hz, $^{4}J_{HH}$ = 3.2 Hz, 4H, $H_{(1)}$), 7.17 (t, $^{3}J_{HH}$ = 7.6 Hz, 2H, $H_{(14)}$), 1.98 – 1.91 (m, 8H, PC$\underline{H}$(CH$_3$)$_2$), 1.87 – 1.78 (m, 8H, PC$\underline{H}$(CH$_3$)$_2$), 1.29 (vdt, $^{3}J_{HH}$ = 6.9 Hz, $^{3,5}J_{HP}$ = 6.9 Hz, 24H, PCH(C$\underline{H}_3$)$_2$), 1.26 (vdt, $^{3}J_{HH}$ = 7.4 Hz, $^{3,5}J_{HP}$ = 7.2 Hz, 24H, PCH(C$\underline{H}_3$)$_2$), 1.20 (vt, $^{2,4}J_{HP}$ = 3.2 Hz, 24H, PC$\underline{H}_3$), 1.09 (vdt, $^{3}J_{HH}$ = 6.9 Hz, $^{3,5}J_{HP}$ = 6.9 Hz, 24H, PCH(C$\underline{H}_3$)$_2$), 0.99 (vdt, $^{3}J_{HH}$ = 6.9 Hz, $^{3,5}J_{HP}$ = 7.0 Hz, 24H, PCH(C$\underline{H}_3$)$_2$). $^{31}$P {$^{1}$H} NMR (162 MHz, C6D6): δ [ppm] = 28.25 (s). $^{13}$C {$^{1}$H} NMR (151 MHz, $C_6D_6$): δ [ppm] = 208.6 (t, $^{2}J_{CP}$ = 14.5 Hz, $\underline{C}$O), 176.9 (s, $C_{(10)}$), 161.9 (t, $^{2}J_{CP}$ = 11.7 Hz, $C_{(9)}$), 135.1 (s, $C_{(6)}$), 134.7 (s, $C_{(11)}$), 132.3 (s, $C_{(13)}$), 131.7 (s, $C_{(3)}$), 131.1 (t, $^{3}J_{CP}$ = 3.1 Hz, $C_{(8)}$), 130.8 (s, $C_{(5)}$), 129.3 (s, $C_{(12)}$), 129.1 (s, $C_{(2)}$), 127.6 (s, $C_{(14)}$), 125.1 (s, $C_{(1)}$), 123.3 (s, $C_{(4)}$), 121.1 (s, $C_{(7)}$), 26.0 (vt, $^{1,3}J_{CP}$ = 12.1 Hz, P$\underline{C}$H(CH$_3$)$_2$), 24.9 (vt, $^{1,3}J_{CP}$ = 12.1 Hz, P$\underline{C}$H(CH$_3$)$_2$), 18.7 (s, PCH(C$\underline{H}_3$)$_2$), 18.3 (s, PCH(C$\underline{H}_3$)$_2$), 17.9 (s, PCH(C$\underline{H}_3$)$_2$), 17.5 (s, PCH(C$\underline{H}_3$)$_2$), 3.3 (vt, $^{1,3}J_{CP}$ = 13.3 Hz, P$\underline{C}$H$_3$). HRMS (ESI) ($CH_2Cl_2$): *m/z* calcd. for $Ru_4P_8C_{112}H_{168}O_{12}^{2+}$ ($M^{2+}$) 1179.8334, found 1179.8097.

## 2.3. Electrochemical and spectroelectrochemical measurements

All electrochemical experiments were performed in a custom-made cylindrical vacuum-tight single-compartment cell. A coiled Pt wire and a coiled Ag wire act as the counter and reference electrodes. They were sealed into glass capillaries and are introduced *via* quickfit screws at opposite sides of the cell. A platinum electrode was used as the working electrode and inserted through the top port *via* a Teflon screw cap with a suitable fitting. The working electrode was polished first with 1 μm and then 0.25 μm diamond pastes (Buehler-Wirtz) before measurements. The cell can be attached to a conventional *Schlenk* line *via* a side arm equipped with a Teflon screw valve and allows experiments to be performed under an atmosphere of argon with approximately 5 mL of analyte solution. $CH_2Cl_2$ / $^n$Bu$_4$N$^+$ BArF$_{24}^-$ (0.1 M) was used as the supporting electrolyte. Referencing was done by adding an equimolar amount of cobaltocenium hexafluorophosphate as an internal standard to the analyte solution after all data of interest had been collected. Representative sets of scans were repeated with the added standard. The final referencing was done against the ferrocene/ferrocenium ($Cp_2Fe^{0/+}$) redox couple with $E_{1/2}$ ($Cp_2Co^{+/0}$) = −1340 mV vs $Cp_2Fe^{0/+}$ for $CH_2Cl_2$ / $^n$Bu$_4$N$^+$ BArF$_{24}^-$. Electrochemical data were acquired with a computer-controlled BASi potentiostat.

The OTTLE cell for spectroelectrochemical experiments was also self-constructed and follows the design of Hartl *et al.* [53]. It comprises of Pt-mesh working and counter electrodes and a thin silver wire as a pseudoreference electrode. The electrodes are sandwiched in between two $CaF_2$ windows of a conventional liquid IR cell. The working electrode was positioned in the center of the spectrometer beam. The required potential was applied by connecting the cell leads to a Wenking POS2 potentiostat by Bank Elektronik-Intelligent Controls GmbH. As supporting electrolyte, a 0.2 M solution of $^n$Bu$_4$N$^+$ PF$_6^-$ in 1,2-$C_2H_4Cl_2$ was used. FT-IR spectra were recorded using a Bruker Tensor II FT-IR spectrometer. UV/Vis/NIR spectra were acquired on a TIDAS fiber optic diode-array spectrophotometer (combined MCS UV/NIR and PGS NIR instrumentation) from j&m Analytik AG.

EPR spectra were obtained using a MiniScope MS 400 X-band tabletop spectrometer by Magnettech GmbH. All measurements were performed at room temperature. Samples of the respective oxidized complexes were generated by using 0.2 equiv. of ferrocenium hexafluorophosphate (monocation) or 2.1 equiv. of acetylferrocenium hexafluoroantimonate (dication) as oxidizing agents. Simulation of experimental EPR spectra was performed with the MATLAB EasySpin program [54].

## 2.4. Computational details

The ground state electronic structures of the full models of all compounds were calculated by density functional theory (DFT) methods using the Gaussian 16 program packages [55]. Geometry optimization followed by vibrational analysis was performed in solvent media. Solvent effects were described by the polarizable continuum model (PCM) with standard parameters for 1,2-dichloroethane [56,57]. The 6–31G(d) polarized double-ζ basis sets [58] were employed for all atoms together with the Perdew, Burke, Ernzerhof exchange and correlation functional (pbe0pbe) [59,60]. The GaussSum program package was used to analyze the results [61], while the visualization of the results was performed with the Avogadro program package [62]. Graphical representations of molecular orbitals were generated with the help of GNU Parallel [63] and plotted using the vmd program package [64] in combination with POV-Ray.

## 2.5. X-Ray crystallography

X-Ray diffraction analysis was performed on a *STOE IPDS II* diffractometer with a graphite-monochromator, and a MoKα-radiation source (λ = 0.71073 Å) at a scan rate of 3 - 30° min$^{-1}$ in ω at $T$ = 100.15 K. Using *Olex2* [65], the structure was solved with the *ShelXT* [66] structure solution program and refined with the ShelXL [67] refinement package using the *Full-Matrix-Least-Squares* method. For visualization,

the *Platon* [68] and *Mercury* [69] programs were used. CCDC 2,337,548 and CCDC 2,337,549 contain the supplementary crystallographic data for this paper. This data can be obtained free of charge *via* www.ccdc.cam.ac.uk/data_request/cif, by emailing data_request@ccdc.cam.ac.uk, or by contacting The Cambridge Crystallographic Data Centre, 12 Union Road, Cambridge CB21EZ, UK; fax: +44 1223 336,033.

### 2.6. Mass spectroemetry

Mass spectra were recorded on an *UHR-TOF Bruker Daltonik maXis plus* ESI-quadrupole time-of-flight (qToF) spectrometer (München, Germany). The resolution is at least 60,000 FWHM at an *m/z* range of singly charged peaks of up to 2700 Da. The detection was performed in positive ion mode with a source voltage of 3.5 kV and a flow rate of 180 µL/h. Nitrogen was used as drying gas. For solvent removal, the temperature was set to 180 °C and the temperature of the spray gas was 20 °C. The calibration was done prior to each measurement by direct infusion of low-concentrated *Agilent ESi-TOF* tuning mixture.

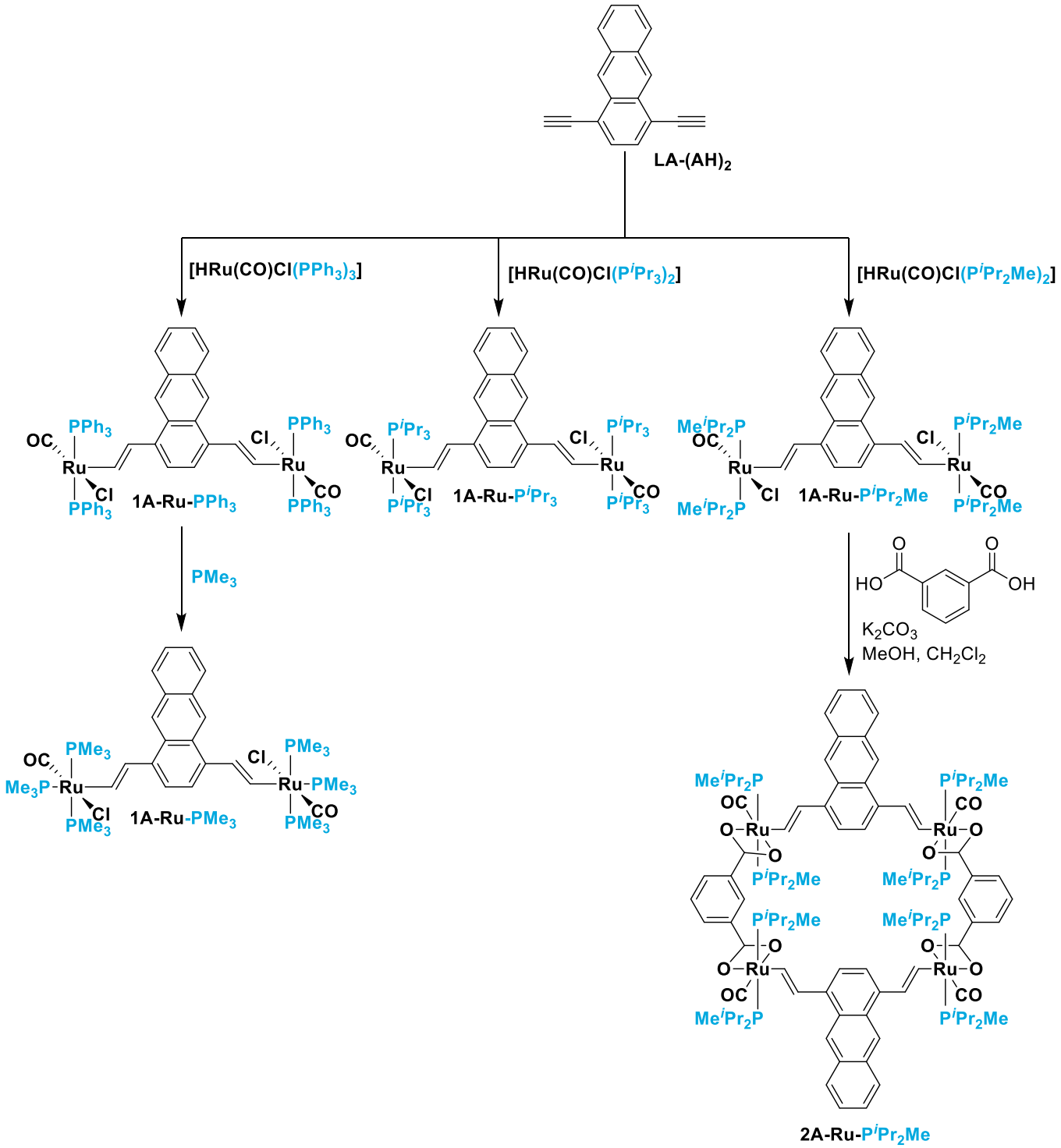


**Scheme 1.** Synthesis pathways for **1A-Ru-P$^i$Pr$_3$**, **1A-Ru-PPh$_3$**, **1A-Ru-PMe$_3$**, **1A-Ru-P$^i$Pr$_2$Me**, and metallamacrocycle **2A-Ru-P$^i$Pr$_2$Me**.

## 3. Results and discussion

### 3.1. Synthesis and characterization

Scheme 1 shows the four anthrylene-bridged diruthenium complexes as well as the tetranuclear metallamacrocycle **2A-Ru-P$^i$Pr$_2$Me** of this study. Complexes **1A-Ru-PMe$_3$** and **1A-Ru-PPh$_3$** were already reported by Liu and coworkers; the $PPh_3$ complex was however only used as a reaction intermediate and was not characterized further [21]. The general synthesis protocol employs twofold hydroruthenation [33] of the terminal dialkyne **LA-(AH)$_2$** [50], using two equivalents of the respective hydride complex [40,51,52]. This provided the bis(alkenyl) complexes **1A-Ru-P$^i$Pr$_3$, 1A-Ru-PPh$_3$**, and **1A-Ru-P$^i$Pr$_2$Me** as red solids in isolated yields of 93%, 90%, and 79%, respectively. When reacted with ten equivalents of $PMe_3$, **1A-Ru-PPh$_3$** afforded yellow crystalline **1A-Ru-PMe$_3$** in 83% yield [21]. Macrocyclic complex **2A-Ru-P$^i$Pr$_2$Me** was obtained in a rather mediocre yield of 10% by adding a methanolic solution of isophtalic acid and potassium carbonate base to a solution containing equimolar amounts of **1A-Ru-P$^i$Pr$_2$Me**. In this case, substantial amounts of insoluble, presumably linear oligomeric byproducts were observed. Better yields of metallamacrocyclic complexes are usually obtained on warming such reaction mixtures, which helps to convert kinetically trapped oligomeric species into the thermodynamically preferred macrocyclic structures. This was, however, not possible here due to inherent thermal instability of **2A-Ru-P$^i$Pr$_2$Me**. Detailed procedures, reaction schemes and characterization data as well as NMR ($^1$H, $^{13}$C{$^1$H} and $^{31}$P{$^1$H}) and mass spectra are provided in the Experimental section and the Supporting Information (Scheme S1 and Figures S1 to S19). Selected NMR data are summarized in Table 1. Compounds **1A-Ru-P$^i$Pr$_3$** and **1A-Ru-PMe$_3$** are stable towards moisture and air, whereas **1A-Ru-PPh$_3$** and **1A-Ru-P$^i$Pr$_2$Me** decompose slowly, even when stored as solids under nitrogen and protected against light, and considerably more rapidly in solution. Tetranuclear metallamacrocycle **2A-Ru-P$^i$Pr$_2$Me** is stable in the solid state, but suffers from gradual degradation in solution.

In agreement with the literature data, the $^{31}$P{$^1$H} spectrum of **1A-Ru-PMe$_3$** exhibits a doublet at $\delta = -7.01$ ppm with $^2J_{PP} = 22.9$ Hz for the axially and a triplet at $\delta$ = -19.28 ppm for the equatorially coordinated $PMe_3$ ligands. The other three complexes with five-coordinated ruthenium ions show one sharp singlet resonance with chemical shifts $\delta$ of 29.46 to 37.74 ppm. Coordinative saturation in metallamacrocycle **2A-Ru-P$^i$Pr$_2$Me** shifts the $^{31}$P{$^1$H} resonance by 1.2 ppm to higher field. Shifts of similar magnitude were found for other pairs of dinuclear and macrocyclic complexes with respective coordination numbers of five and six [45,70,71]. In the $^1$H NMR spectra, the $\alpha$ and $\beta$ vinyl protons give rise to two doublet resonances at $\delta = 9.30 - 8.19$ ppm and $\delta = 7.73 - 6.61$ ppm; both these resonances are shifted to lower field in coordinatively saturated **2A-Ru-P$^i$Pr$_2$Me** when compared to its 16 VE precursor **1A-Ru-P$^i$Pr$_2$Me**. $^3J_{HH}$ coupling constants of 12.4 – 17.8 Hz indicate *trans* configuration at the olefinic double bonds. The single set of vinylic resonances in the $^1$H NMR spectrum of **2A-Ru-P$^i$Pr$_2$Me** confirms its cyclic structure. The $^{13}$C resonance signal of the carbonyl C atom is split into a triplet, or in the case of **1A-Ru-PMe$_3$** a doublet-of-triplet and resonates at $\delta = 208.6 - 203.1$ ppm with $^2J_{CP} = 11.4 - 14.5$ Hz. In agreement with previous observations, the $^{13}$C{$^1$H} CO resonance signal is shifted downfield by approximately 5 ppm in **2A-Ru-P$^i$Pr$_2$Me** as compared to **1A-Ru-P$^i$Pr$_2$Me** [45,70,71]. The poor solubility of **1A-Ru-PPh$_3$** prevented us from recording useful $^{13}$C{$^1$H} NMR spectra. Ultrahigh-resolution mass spectrometry (UHR ESI MS) confirmed the tetranuclear structure of **2A-Ru-P$^i$Pr$_2$Me** by virtue of its $[M]^{2+}$ mass peak at 1179.8097 amu (calculated value: 1179.8334 amu) with half-integer spacings for the individual isotopomers (see Figure S19 of the Supporting Information).

Single crystals of complexes **1A-Ru-P$^i$Pr$_3$** and **1A-Ru-PMe$_3$** that were suitable for X-ray diffractometry were obtained by slow diffusion of $^n$pentane into a saturated solution of **1A-Ru-P$^i$Pr$_3$** or from diethyl ether, respectively. The molecular structures are shown in Fig. 1 and Figure S22 of the Supporting Information; selected bond parameters and interplanar angles of **1A-Ru-PMe$_3$** are summarized in Table 2. Details to the data collection, structure solution, and refinement, as well as listings of atomic coordinates and displacement parameters are provided in Tables S1 – S4 of the Supporting Information. Liu and coworkers have already determined the molecular structure of **1A-Ru-PMe$_3$** from single crystals of its $CH_2Cl_2$ solvate grown from a dichloromethane / $^n$hexane mixture [21]. Having crystallized in the same space group *C*2/*c*, the present structure obtained from solvent-free crystals closely resembles the earlier one and shows only subtle differences (see Table 2).

The six-coordinated ruthenium atoms adopt a distorted octahedral coordination geometry with a meridional arrangement of the three $PMe_3$ ligands, thereby preserving the favorable *trans*-arrangement of the Cl $\pi$-donor and the CO $\pi$-acceptor ligands. Deviations from a perfect octahedral arrangement consist in an opening of the P-Ru-P$_{cis}$ angles to 94.10 (3) or 100.85(3)° and a concomitant compression of the P-Ru-P$_{trans}$ angles to 163.45(3) or 165.12(3)°. The same holds for the angles spanned by the alkenyl carbon atoms C(1) and C(18), the ruthenium ions and the *cis*-disposed phosphine atoms, which range from 81.47(7) to 86.99(8)°. As the combined result of a lower bond order and the larger atomic radius of a sp$^2$ as compared to a sp hybridized carbon atom, the bonds between the ruthenium atoms and the vinyl carbon atoms (Ru(1)-C(1) = 2.098(2) Å, Ru(2)-C(18) = 2.098(2) Å) are appreciably longer than the bonds Ru(1)-C(19) (1.818(4) Å) and Ru(2)-C(20) (1.822(3) Å) to the carbonyl C atoms. The lengthening of Ru-P bonds to the equatorial $PMe_3$ ligands by ca. 5 pm when compared to the axial ones is a recurrent pattern in complexes of this type and results from their positioning opposite to the strongly *trans*-influencing alkenyl donor [15,16,29,42,72,73]. In both structures, the Ru-CH=CH units are rotated to different sides out of the anthracene plane. In the present structure, the torsion angles of 42.63° and 26.05° differ substantially, whereas they adopted more similar values of 39.50° and 32.07° in the previous structure.

Space-filling models of both structures of **1A-Ru-PMe$_3$** show that, in spite of the extended $\pi$-perimeter of the 1,4-disubstituted anthrylene ligand, the sterically demanding complex moieties leave little free space for $\pi$-stacking. As a consequence, intermolecular interactions are confined to C-H···$\pi$ interactions to three methyl protons of $PMe_3$ ligands that belong to molecules situated above and below (see Figures S20 and S21 of the Supporting Information). In the present structure, these contacts range from 2.662 to 2.783 Å. Only two longer contacts of 2.813 and 2.831 Å are found in the dichloromethane monosolvate, where they are augmented by an additional C-H···$\pi$ interaction to a proton of the $CH_2Cl_2$ solvate molecule. In the crystal, neighboring molecules in the *ab* plane are alternately tilted in opposite directions with their anthracene planes disposed at an interplanar angle of 40.06° (see Figure S20 of the Supporting Information); in the previous structure this angle is slightly smaller at 38.10°

**Table 1**
Selected $^{31}$P{$^1$H}, $^1$H, and $^{13}$C{$^1$H} spectroscopic data for **1A-Ru-P$^i$Pr$_3$, 1A-Ru-PPh$_3$, 1A-Ru-PMe$_3$, 1A-Ru-P$^i$Pr$_2$Me,** and the tetranuclear metallamacrocycle **2A-Ru-P$^i$Pr$_2$Me**.

| | *P*R$_2$R' | Ru-C*H* ($^3J_{HH}$) | Ru-CH=C*H* ($^3J_{HH}$) | $C_{CO}$ ($^2J_{CP}$) |
|---|---|---|---|---|
| **1A-Ru-P$^i$Pr$_3$**[b] | 37.74 | 9.03 (12.8) | 7.40 (12.8) | 204.1 (13.2) |
| **1A-Ru-PMe$_3$**[a] | −7.01, −19.28 | 8.19 (17.8) | 7.49 (17.8) | 203.1 (13.2, 11.4) |
| **1A-Ru-PPh$_3$**[a] | 31.39[b] | 8.51 (12.6) | 6.61 (12.6) | -[c] |
| **1A-Ru-P$^i$Pr$_2$Me**[b] | 29.46 | 8.76 (12.4) | 7.27 (12.4) | 203.5 (12.7) |
| **2A-Ru-P$^i$Pr$_2$Me**[b] | 28.25 | 9.30 (15.0) | 7.73 (15.0) | 208.6 (14.5) |

[a] Measured in $CD_2Cl_2$.
[b] Measured in $C_6D_6$.
[c] Not observed due to poor solubility.

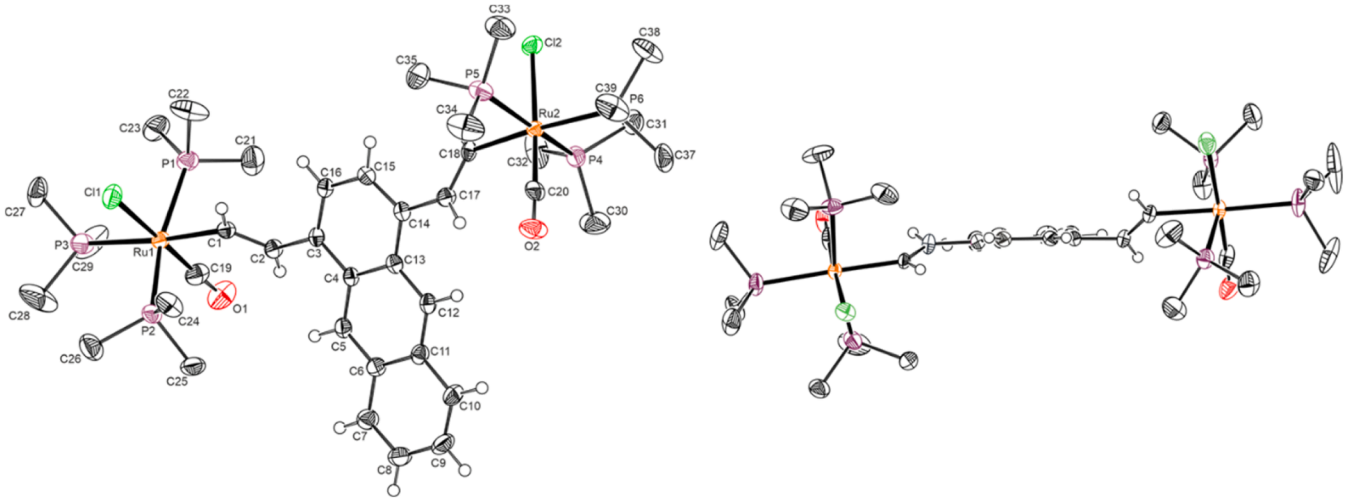


**Fig. 1.** Left: ORTEP of the molecular structure of **1A-Ru-PMe$_3$** in the crystalline state. Hydrogen atoms of the phosphine ligands are omitted for reasons of clarity. Ellipsoids are displayed at the 50 % probability level. Right: Side-view of the molecular structure of **1A-Ru-PMe$_3$**.

**Table 2**
Selected bond lengths [Å], bond angles [°], and dihedral angles [°] from the crystal structure of **1A-Ru-PMe$_3$**.

| | | **1A-Ru-PMe$_3$** | |
|---|---|---|---|
| | | this work | ref. [21] |
| bond lengths [Å] | Ru(1)-P(1) | 2.3583(8) | – |
| | Ru(1)-P(2) | 2.3621(8) | – |
| | Ru(1)-P(3) | 2.4116(7) | 2.4135(7) |
| | Ru(1)-C(1) | 2.098(2) | 2.098(2) |
| | Ru(1)-C(19) | 1.818(4) | 1.826(4) |
| | C(1)-C(2) | 1.336(4) | 1.333(4) |
| | C(2)-C(3) | 1.473(3) | 1.479(3) |
| | C(14)-C(17) | 1.474(3) | 1.482(3) |
| | C(17)-C(18) | 1.335(4) | 1.335(4) |
| | Ru(2)-C(18) | 2.098(2) | 2.099(2) |
| | Ru(2)-C(20) | 1.822(3) | 1.810(3) |
| | Ru(2)-P(4) | 2.3587(8) | – |
| | Ru(2)-P(5) | 2.3444(8) | – |
| | Ru(2)-P(6) | 2.3857(7) | 2.4010(7) |
| bond angles [°] | P(1)-Ru(1)-P(2) | 163.45(3) | 166.20(3) |
| | P(1)-Ru(1)-C(1) | 81.74(7) | – |
| | P(2)-Ru(1)-C(1) | 82.00(7) | – |
| | P(3)-Ru(1)-C(1) | 174.55(8) | 176.73(7) |
| | Ru(1)-C(1)-C(2) | 174.55(8) | 130.83(19) |
| | C(1)-Ru(1)-C(19) | 90.98(12) | – |
| | C(1)-Ru(1)-Cl(1) | 87.33(8) | – |
| | C(1)-C(2)-C(3) | 125.1(3) | 125.1(2) |
| | C(14)-C(17)-C(18) | 126.6(2) | 125.5(3) |
| | C(18)-Ru(2)-C(20) | 89.11(11) | – |
| | C(18)-Ru(2)-Cl(2) | 89.21(8) | |
| | C(17)-C(18)-Ru(2) | 129.2(2) | 130.3(2) |
| | P(6)-Ru(2)-C(18) | 175.70(8) | 177.278) |
| | P(5)-Ru(2)-C(18) | 86.99(8) | – |
| | P(4)-Ru(2)-C(18) | 82.85(8) | – |
| | P(4)-Ru(2)-P(5) | 165.15(3) | 165.12(3) |
| dihedral angles [°] | plane [Ru(1)-C(1)-C(2)] plane [C(3)-C(16)-C(15)] | 42.63 | 39.50 |
| | plane [C(14)-C(15)-C(16)] plane [C(17)-C(18)-Ru(2)] | 26.05 | 32.07 |
| | plane [Ru(1)-C(1)-C(2)] plane [C(17)-C(18)-Ru(2)] | 66.19 | 64.49 |

**1-Ru-P$^i$Pr$_3$** crystallized in space group $P3_2$. A plot of the crystallographically determined molecular structure with the atomic numbering is shown in Figure S22 of the Supporting Information. A somewhat poor crystal quality and disorder of the $^i$Pr substituents at the phosphine ligands render the interatomic bond lengths and angles too imprecise to allow for meaningful discussion of bond parameters so that only the gross features are mentioned. The five-coordinated ruthenium ions adopt the usual distorted square pyramidal coordination geometry with the alkenyl ligand at the apical site and *trans*-disposed phosphine ligands in the pyramid base. Like in **1A-Ru-PMe$_3$**, the two appended ruthenium alkenyl moieties are rotated in opposite directions out of the anthracene plane; interplanar angles between the plane Ru-CH=CH and the latter amount to 29.1° and 32.5° In the crystalline state, individual molecules with equivalent orientation interconnect to stepped, staircase-like sheets *via* short C—H···Cl contacts of 2.64 and 2.73 Å between $^i$Pr methine protons and the chlorido ligands. Adjacent sheets have their anthracene planes inclined by 48.2° and interconnect through C—H···O hydrogen bonds of 2.353 Å and 2.618 Å as well as CH···π interactions to the alkenyl β carbon atom C2 and anthryl C atom C4 of 2.817 Å and 2.782 Å. In each instance, $^i$Pr methyl protons act as the H-bond donors. Packing diagrams can be found in Figure S23 of the Supporting Information.

### 3.2. Electrochemistry

One aim of this study was to investigate, how the $PR_3$ ligands affect the redox potentials of the individual oxidations and the chemical stabilities of the oxidized forms of a divinylarylene-bridged diruthenium complex with a π-extended arylene linker. To these ends, all four dinuclear complexes as well as **2A-Ru-P$^i$Pr$_2$Me** were subjected to cyclic and square wave voltammetric measurements in a 0.1 M solution of $^n$Bu$_4$N$^+$ BArF$_{24}^-$ in $CH_2Cl_2$ (BArF$_{24}^-$ = [B{C$_6$H$_3$(CF$_3$)$_2$-3,5}$_4$]$^-$) as the electrolyte. The $CF_3$-substituted tetraarylborate counterion was chosen in order to minimize ion pairing effects and to enhance the stability of the electrophilic oxidation products by providing a very weakly nucleophilic environment [74–78]. The results are shown in Fig. 2 and Figures S24 – S29 of the Supporting Information, while pertinent data are collected in Table 3.

All diruthenium complexes display two consecutive, well-separated one-electron oxidations. Half-wave potential differences of 202 – 336 mV and the corresponding $K_c$ values of $2.6{\cdot}10^3$ to $4.8{\cdot}10^5$ indicate that the one-electron oxidized mixed-valent radical cations are reasonably stable with respect to disproportionation (Equation 1; $c^{n+}$ = concentration of the compound in oxidation state $n+$, $F$ = Faraday's constant, $R$ gas constant). The half-wave potentials $E_{1/2}$ of the corresponding redox processes follow the ordering P$^i$Pr$_3$ < P$^i$Pr$_2$Me ≤ PMe$_3$ < PPh$_3$, which agrees with the different electron-donating properties of the phosphine ligands [81–83]. Despite their lower valence electron count of 16, complexes **1A-Ru-P$^i$Pr$_3$** and **1A-Ru-P$^i$Pr$_2$Me** are easier to oxidize than **1A-Ru-PMe$_3$**. The data in Table 3 also show that the phosphine ligands exert a larger influence on the half-wave potential of the second than of

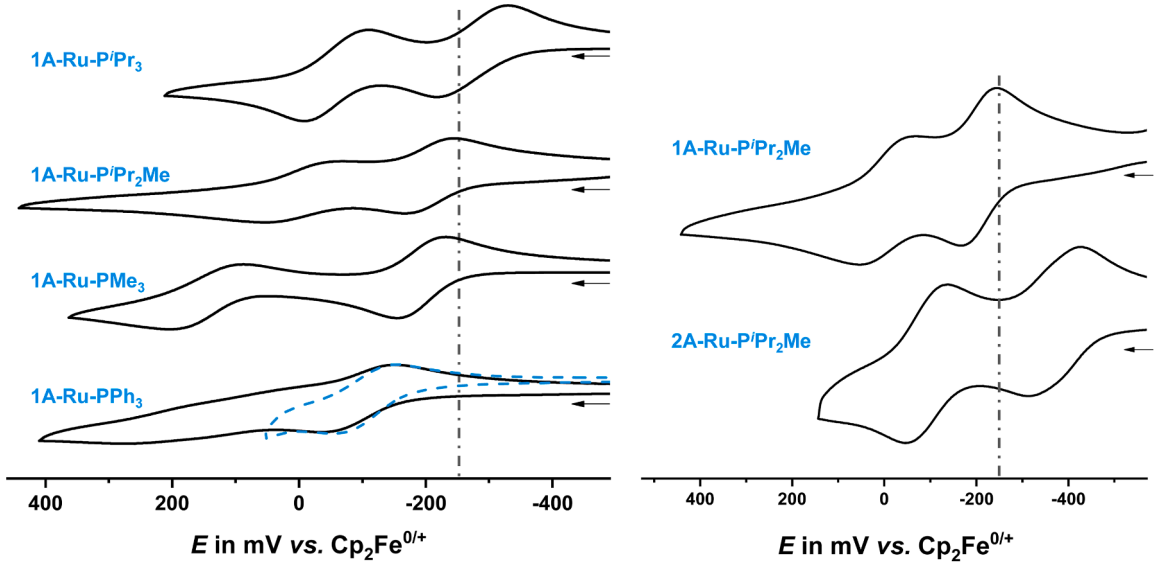


**Fig. 2.** Cyclic voltammograms of **1A-Ru-P$^i$Pr$_3$, 1A-Ru-P$^i$Pr$_2$Me, 1A-Ru-PMe$_3$**, and **1A-Ru-PPh$_3$** (left) and of **1A-Ru-P$^i$Pr$_2$Me** and **2A-Ru-P$^i$Pr$_2$Me** (right) at $\nu = 100$ mV/s in $^n$Bu$_4$N$^+$ BArF$_{24}^-$ / $CH_2Cl_2$; dotted gray lines at −250 mV serve as guide to the eye.

**Table 3**
Half-wave potentials of **1A-Ru-P$^i$Pr$_3$, 1A-Ru-PMe$_3$, 1A-Ru-PPh$_3$, 1A-Ru-P$^i$Pr$_2$Me, 2A-Ru-P$^i$Pr$_2$Me**, and the 1,4-phenylene- and 1,4-naphthylene-bridged analogs **Ph-Ru-P$^i$Pr$_3$** and **NA-Ru-P$^i$Pr$_3$** in 0.1 M $CH_2Cl_2$ / $^n$Bu$_4$N$^+$ BArF$_{24}^-$ at r.t. Half-wave potentials $E_{1/2}$ and peak potential differences $\Delta E_p$ are given in mV; $E_{1/2}$ values are calibrated against the Cp$_2$Fe$^{0/+}$ standard ($E_{1/2} = 0$ mV).

| | $E_{1/2}0^{/+}$ ($\Delta E_p$) | $E_{1/2}^{+/2+}$ ($\Delta E_p$) | $E_{1/2}^{2+/3+}$ ($\Delta E_p$) | $E_{1/2}^{3+/4+}$ ($\Delta E_p$) | $\Delta E_{1/2}$ |
|---|---|---|---|---|---|
| **1A-Ru-P$^i$Pr$_3$** | −250 (111) | −27 (100) | – | – | 223 |
| **1A-Ru-P$^i$Pr$_2$Me** | −192 (75) | 10 (110) | – | – | 202 |
| **1A-Ru-PPh$_3$** | −92 (109) | 204 (n.a.) | – | – | 296 |
| **1A-Ru-PMe$_3$** | −184 (73) | 152 (113) | – | – | 336 |
| **2A-Ru-P$^i$Pr$_2$Me** | −403[a] (109) | −325[a] (109) | −93 (91) | −93 (91) | 271[b] |
| **Ph-Ru-P$^i$Pr$_3$**[c] | −180 (72) | 130 (74) | – | – | 310 |
| **NA-Ru-P$^i$Pr$_3$**[d] | −235 (74) | 110 (75) | – | – | 345 |

[a] Determined by deconvolution of square wave voltammograms.
[b] Difference between the half-wave potential of the 2+/4+ and the average value of the 0/+ and +/2+ redox couples.
[c] From ref. [79].
[d] From ref. [80].

the first oxidation.

$$K_{comp} = \frac{(c^+)^2}{c^0 \cdot c^{2+}} = exp^{\frac{nF\Delta E_{1/2}}{RT}} \quad (1)$$

Only for the particularly electron-rich complex **1A-Ru-P$^i$Pr$_3$** with the sterically most demanding phosphine ligands, both oxidations are chemically reversible on the voltammetric timescale. Replacement of just one propyl group for methyl in **1A-Ru-P$^i$Pr$_2$Me** renders the second oxidation only partially reversible. The same holds for **1A-Ru-PMe$_3$**. Chemical follow processes are evidenced by additional voltammetric peaks that appear after repetitive cycling over both waves (see Figure S26 and S27 of the Supporting Information). With the less donating $PPh_3$ ligands, even the first oxidation of **1A-Ru-PPh$_3$** is chemically only partially reversible, while the second oxidation appears to be almost irreversible, so that the potentials were determined from the peaks in square wave voltammetry. For the latter complex, increasing the sweep rate leads to even larger deviations from ideality, which suggests that the odd appearance of particularly the second oxidation is also caused by sluggish electron transfer kinetics. The same holds, although to a lesser degree, for complexes **1A-Ru-P$^i$Pr$_2$Me** and **1A-Ru-PMe$_3$**, which also show a broadening of the +/2+ wave and decreased peak currents for this process in square-wave voltammetry (see Figure S25 and S27 of the Supporting Information).

In metallamacroycle **2A-Ru-P$^i$Pr$_2$Me** with mutually insulated sides of the general type present in **1A-Ru-P$^i$Pr$_2$Me**, yet with coordinatively saturated ruthenium entities, the number of electrons involved in every redox process doubles to two. Coordinative saturation lowers the half-wave potentials by ca. 200 and 315 mV for the first and second oxidations, improves the chemical stabilities of the oxidized forms and removes the kinetic complications of the higher oxidations. The larger overall breadth of the first oxidation wave is the result of a 78 mV difference between the half-wave potentials for the first oxidation of the divinylanthrylene-diruthenium sides as determined by deconvolution of the square-wave peak. This splitting is rooted in electrostatic interactions [70].

Complex **1A-Ru-P$^i$Pr$_3$** extends the series of 1,4-phenylene-bridged [1,79] and 1,4-naphthylene-bridged [80] diruthenium complexes **Ph-Ru-P$^i$Pr$_3$** and **NA-Ru-P$^i$Pr$_3$** with the same ligand set to the next congener with an additional phenyl ring condensed to the arylene linker (Fig. 3). The progressive shifting of the half-wave potentials to lower values reflects increasing bridge contributions to the individual redox processes, owing to the increasing energetic stabilization of the relevant π-orbitals. Similar observations were reported for a closely related series of diruthenium complexes with appended Cp*(dppe)Ru-C≡C- entities (Cp* = $\eta^5$-$C_5Me_5$, dppe = 1,2-bis(diphenylphosphino)ethane, $Ph_2P$-$C_2H_4$-$PPh_2$, see Fig. 3) [84].

### 3.3. The oxidized forms: aspects of electron- and spin-density distributions in the mixed-valent states as probed by spectroelectrochemistry

Divinylarylene-bridged diruthenium complexes with {Ru(CO)$(PR_3)_nL$} entities are particularly well-suited to address the questions about metal and ligand contributions to the so-called redox orbitals and the extent of intrinsic electron delocalization in their one-electron oxidized, mixed-valent states. The overall shift of the CO stretching bands provides a sensitive measure for metal contributions to the respective oxidations, while the CO band pattern mirrors the degree of intrinsic electron delocalization. In order to address this issue, we generated the various oxidized forms by electrolysis inside an optically

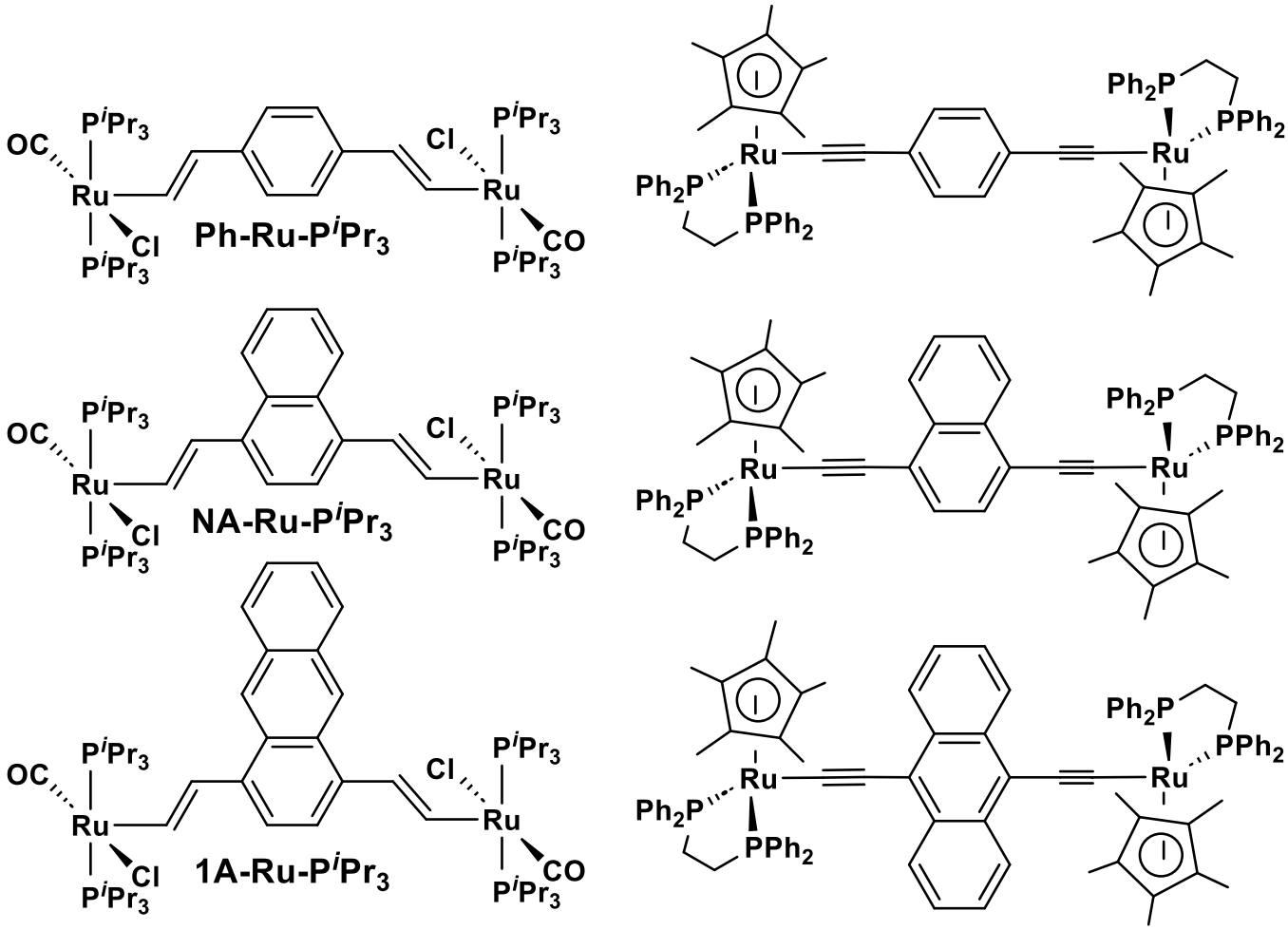


**Fig. 3.** Structures of the two series of phenylene-, naphthylene-, and anthrylene-bridged diruthenium complexes with ethenediyl or ethynediyl connectors.

and IR transparent electrochemical cell [53], as well as by chemical oxidation with a chemoselective oxidizing agent [85], and spectroscopically characterized them by IR, UV/Vis/NIR and EPR spectroscopy. All spectroelectrochemical measurements were performed in 1,2-dichloroethane (DCE) in the presence of 0.2 M $^n$Bu$_4$N$^+$ PF$_6^-$ as the supporting electrolyte.

Fig. 4 illustrates the changes in mid IR spectra induced by stepwise oxidation of **1A-Ru-P$^i$Pr$_3$** in our OTTLE cell as a representative example, while Fig. 5 gives an overview over all complexes (for the results on **2A-Ru-P$^i$Pr$_2$Me** and more details, see Figures S30 – S37 of the Supporting Information). Relevant data from these studies are collected in Table 4. In spite of the non-idealities observed in cyclic and square-wave

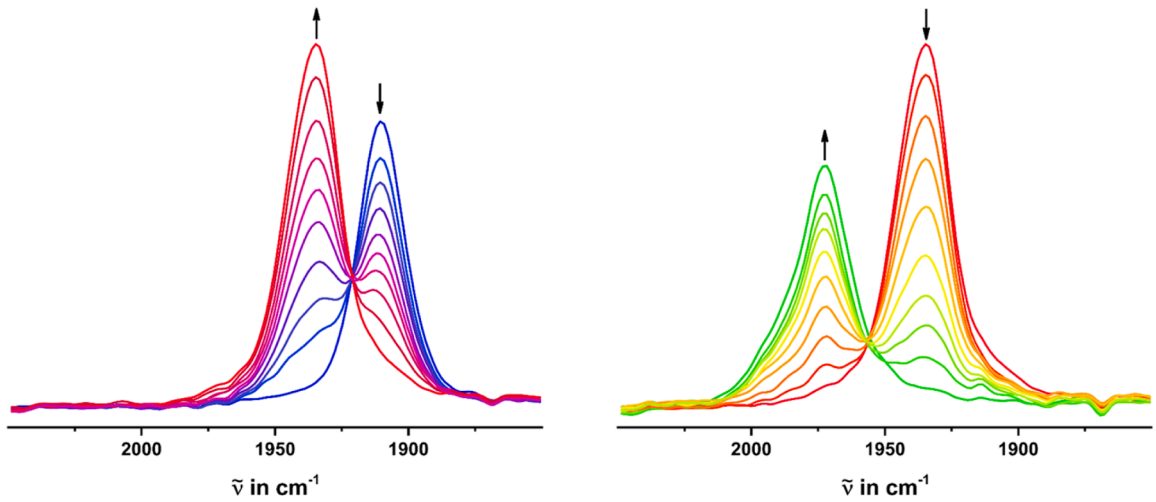


**Fig. 4.** Changes of the IR spectra during electrochemical oxidation of **1A-Ru-P$^i$Pr$_3$** to its radical cation (left) and during further oxidation to the corresponding dication (right) in 0.2 M 1,2-$C_2H_4Cl_2$ / $^n$Bu$_4$N$^+$ PF$_6^-$ at r.t.

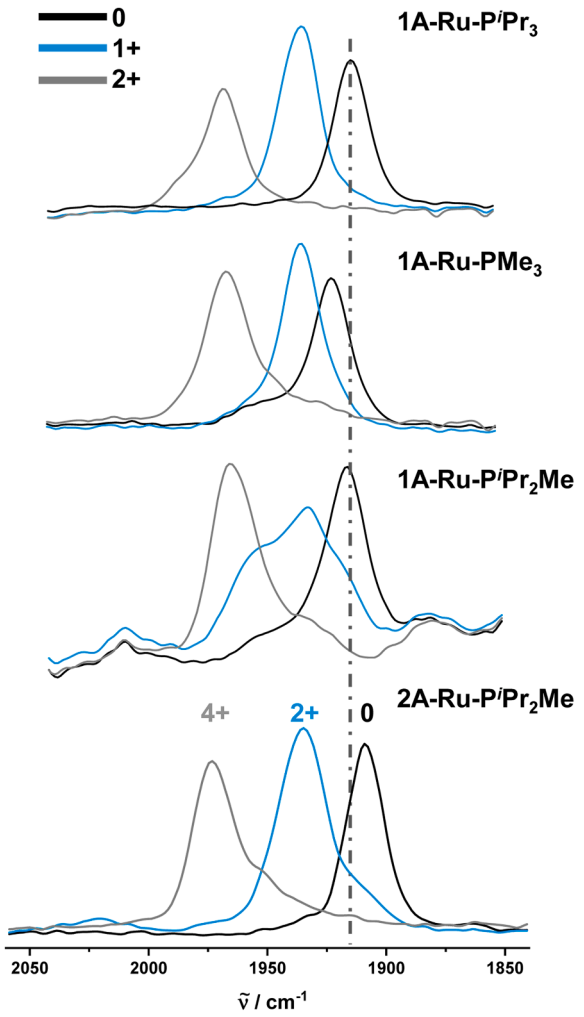


**Fig. 5.** Evolution of the ν(CO) bands in IR spectra upon stepwise oxidation of **1A-Ru-P$^i$Pr$_3$**, **1A-Ru-PMe$_3$**, **1A-Ru-P$^i$Pr$_2$Me**, and **2A-Ru-P$^i$Pr$_2$Me**.

voltammetry, clean isosbestic points were observed throughout the entire spectroelectrochemical experiments, suggesting uncomplicated transformations devoid of chemical decomposition under these conditions.

In the neutral state, the divinylanthrylene-bridged diruthenium complexes exhibit one single, sharp Ru(CO) band for the out-of-phase combination of the CO stretches. The ordering of band energies, which vary between 1910 cm$^{-1}$ in **1A-Ru-P$^i$Pr$_3$** and 1934 cm$^{-1}$ in **1A-Ru-PPh$_3$**, matches with that of the half-wave potentials obtained from voltammetry studies.

One-electron oxidized, mixed-valent **1A-Ru-P$^i$Pr$_3^{\bullet+}$**, **1A-Ru-PMe$_3^{\bullet+}$**, and **2A-Ru-P$^i$Pr$_2$Me$^{\bullet\bullet 2+}$** retain the pattern of only a single CO band. This means that the two ruthenium moieties remain electronically equivalent and that the mixed-valent species have fully delocalized electronic ground states. **1A-Ru-P$^i$Pr$_2$Me$^{\bullet+}$** however shows a different behavior. A major CO band at 1936 cm$^{-1}$ is flanked by two weaker CO bands located at 1918 cm$^{-1}$ and 1961 cm$^{-1}$. Such behavior is indicative of the coexistence of species with delocalized and localized electronic structures. Similar observations were already reported for the diethynylarylene-bridged diruthenium complexes shown in the right panel of Fig. 3, and found to correspond to species that differ with respect to whether the oxidation has primarily occurred on the bridging ligand (delocalized forms) or one of the ruthenium termini (localized forms). Which of the two possible structures prevails depends on the torsion angles at the Ru-C$_2$H$_n$-arylene connectors ($n$ = 0, 2) [49,84,86,87]. Coplanar structures favor bridge-dominated redox processes and a delocalized electronic ground state [49,84,86,87]. The same may hold here. Thus, an enhanced twisting of one or both vinyl ruthenium entities would confine the charge to the vinylanthryl ruthenium unit with the more coplanar arrangement or one of the ruthenium ions, and hence result in electronic decoupling. In **2A-Ru-P$^i$Pr$_2$Me$^{\bullet\bullet 2+}$** incorporation of the P$^i$Pr$_2$Me-coordinated diruthenium anthrylene unit in a more rigid macrocyclic structure seems to prevent large-amplitude torsions, so that both π-conjugated sides remain intrinsically delocalized. Oxidation of **1A-Ru-PPh$_3$** resulted in irreversible spectroscopic changes indicating chemical decomposition, so that no meaningful IR data can be reported.

**Table 4**
Relevant IR/NIR and UV/Vis/NIR data of the TMA-protected ligand precursor, **1A-Ru-P$^i$Pr$_3$**, **1A-Ru-PMe$_3$**, **1A-Ru-PPh$_3$**, **1A-Ru-P$^i$Pr$_2$Me** and **2A-Ru-P$^i$Pr$_2$Me** in all accessible oxidation states.

| | $\nu_{CO}$ (cm$^{-1}$)[a] | λ (nm) ($\varepsilon_{max}$ ($10^3$ $M^{-1}$cm$^{-1}$))[a] |
|---|---|---|
| **LA-(ATMS)$_2$** | – | 240 (34.5), 270 (83.0), 290 (19.1), 300 (21.8), 375 (9.3), 400 (17.4), 420 (18.2) |
| **1A-Ru-P$^i$Pr$_3$** | 1910 | 330 (19.6), 470 (14.7) |
| **1A-Ru-P$^i$Pr$_3^{\bullet+}$** | 1935 | 335 (17.0), 470 (13.8), 515 (10.8), 790 (15.3), 885 (11.1), 1095 (10.7) |
| **1A-Ru-P$^i$Pr$_3^{2+}$** | 1973 | 400 (13.7), 440 (13.8), 610 (34.2) |
| **1A-Ru-PMe$_3$** | 1921 | 255 (55.7), 290 (28.8), 320 (18.3), 450 (10.8) |
| **1A-Ru-PMe$_3^{\bullet+}$**[b,c] | 1936 | 460 (17.8), 500 (13.2), 620 (15.5), 740 (9.6), 835 (7.7), 1010 (8.2) |
| **1A-Ru-PMe$_3^{2+}$**[b,c] | 1972 | 450 (15.1), 635 (16.5) |
| **1A-Ru-PPh$_3$** | 1934 | 450 (13.1) |
| **1A-Ru-P$^i$Pr$_2$Me** | 1915 | 290 (38.0), 460 (15.1) |
| **1A-Ru-P$^i$Pr$_2$Me$^{\bullet+}$** | 1918, 1936, 1961[d] | 460 (15.6), 520 (13.2), 615 (15.4), 790 (5.4), 890 (2.6), 1120 (3.3) |
| **1A-Ru-P$^i$Pr$_2$Me$^{2+}$** | 1971 | 460 (15.3), 620 (22.8) |
| **2A-Ru-P$^i$Pr$_2$Me** | 1909 | 290 (46.8), 485 (27.9) |
| **2A-Ru-P$^i$Pr$_2$Me$^{\bullet\bullet 2+}$** | 1935 | 445 (28.1), 470 (30.0), 520 (31.4), 780 (45.0), 880 (29.7), 1075 (39.0) |
| **2A-Ru-P$^i$Pr$_2$Me$^{4+}$** | 1973 | 425 (33.6), 445 (34.4), 600 (87.8), 885 (11.0) |

[a] Measured in 1,2-C$_2$H$_4$Cl$_2$ / 0.2 M $^n$Bu$_4$N$^+$ PF$_6^-$ at r.t, if not stated otherwise.
[b] Measured by chemical oxidation with suitable oxidizing agent.
[c] Extinction coefficients may be lower estimates as some decomposition and incomplete electrochemical conversion cannot be ruled out.
[d] Determined by deconvolution.

Interestingly, the valence-delocalized radical cations show nearly the same energy of their CO stretch, ca. 1935 cm$^{-1}$, irrespective of the VE count on the ruthenium ions and the identity of the phosphine ligands. The same also holds for the corresponding dications, which all show a single CO band near 1973 cm$^{-1}$. It thus seems that the extent to which the anthrylene bridge and the ruthenium-coligand entities {Ru(CO)(PR$_3$)$_n$L} contribute to the redox processes vary between the different complexes to result in rather uniform electron density distributions. We note in this vein that the overall CO band shifts $\Delta\tilde{\nu}_{CO}$ of 51 cm$^{-1}$ to 63 cm$^{-1}$ on twofold oxidation fall considerably short of the value of ca. 120 cm$^{-1}$ expected for the loss of a full unit of charge from a ruthenium ion [88]. Such attenuated shifts are tokens of sizable bridge-contributions to the individual oxidations. The latter expectedly increase with progressive bridge annulation as evidenced by the 1,4-phenylene- ($\Delta\tilde{\nu}_{CO}^{0/2+}$ 68 cm$^{-1}$), 1,4-naphthylene- ($\Delta\tilde{\nu}_{CO}^{0/2+}$ = 65 cm$^{-1}$), and 1,4-anthrylene--bridged ($\Delta\tilde{\nu}_{CO}^{0/2+}$= 63 cm$^{-1}$) diruthenium alkenyl complexes shown in the left panel of Fig. 3.

The intrinsically delocalized electronic structures of (di)radical (di) cations **1A-Ru-P$^i$Pr$_3^{\bullet+}$**, **2A-Ru-P$^i$Pr$_2$Me$^{\bullet\bullet 2+}$**, and **1A-Ru-PMe$_3^{\bullet+}$** are also indicated by their EPR hyperfine splitting (hfs) patterns. Hence, **1A-Ru-P$^i$Pr$_3^{\bullet+}$** and **2A-Ru-P$^i$Pr$_2$Me$^{\bullet\bullet 2+}$** show resolved hfs to four equivalent $^{31}$P and two identical $^{99/101}$Ru nuclei, while the experimental EPR spectrum of **1A-Ru-PMe$_3^{\bullet+}$** is well reproduced by assuming identical hfs to the four axial and slightly smaller hfs to the equatorial PMe$_3$ ligands (see Table 5). The EPR spectrum of **1A-Ru-P$^i$Pr$_2$Me$^{\bullet+}$** is suspiciously broad

**Table 5**
EPR parameters for **1A-Ru-P$^i$Pr$_3^{\bullet+}$**, **1A-Ru-PMe$_3^{\bullet+}$**, **1A-Ru-PPh$_3^{\bullet+}$**, **1A-Ru-P$^i$Pr$_2$Me$^{\bullet+}$**, and **2A-Ru-P$^i$Pr$_2$Me$^{\bullet\bullet 2+}$** at 20±3 °C. Hyperfine coupling constants *A* are given in *Gauss* at 20±3 °C.

| | $g_{iso}$(20 °C) | $A(^{99/101}Ru)$ | $A(^{31}P)$ | $A(^{1}H)$ |
|---|---|---|---|---|
| **1A-Ru-P$^i$Pr$_3^{\bullet+}$** | 2.010 | 3.2 (2) | 8.9 (4) | 1.8 (4), 1.4 (2) |
| **1A-Ru-PMe$_3^{\bullet+}$** | 2.006 | 1.8 (2) | 8.6 (4), 7.1 (2) | 1.8 (4), 1.1 (2) |
| **1A-Ru-PPh$_3^{\bullet+}$** | 2.008 | – | – | – |
| **1A-Ru-P$^i$Pr$_2$Me$^{\bullet+}$** | 2.011 | – | – | – |
| **2A-Ru-P$^i$Pr$_2$Me$^{\bullet\bullet 2+}$** | 2.010 | 6.1 (2) | 5.7 (4) | – |

and shows no resolved hfs (see Fig. 6 and Figures S38 – S41 of the Supporting Information). The broad, unstructured resonance signal supports the idea that **1A-Ru-P$^i$Pr$_2$Me$^{\bullet+}$** exists as a mixture of conformers with different electronic structures and a dynamic interconversion between them on the EPR timescale. The finding that **2A-Ru-P$^i$Pr$_2$Me$^{\bullet\bullet 2+}$** with two subunits closely related to **1A-Ru-P$^i$Pr$_2$Me$^{\bullet+}$** is nevertheless spin-delocalized, as revealed by resolved hfs to four equivalent $^{31}$P and two identical $^{99/101}$Ru nuclei, is internally consistent with our IR results (see Fig. 6, bottom). We note that the intermittently formed monocation **2A-Ru-P$^i$Pr$_2$Me$^{\bullet+}$** with one oxidized and one neutral diruthenium divinylanthrylene unit has no specific spectroscopic fingerprints. This proves that the two identical divinylanthrylene diruthenium subunits within this macrocycle are mutually insulated, like it was observed for similar metallamacrocycles with dicarboxylate linkers [46,47,71,89,90].

Attenuated CO band shifts in the IR and the observability of resolved EPR spectra in fluid solution are tokens of large ligand contributions to the molecular orbitals (MOs) that are involved in stepwise electron transfer. One therefore expects that the oxidized forms feature electronic absorption bands akin to anthracenyl (radical) cations. This we probed by UV/Vis/NIR spectroelectrochemistry. The UV/Vis spectra of the neutral complexes are similar with intense bands ($\varepsilon > 10^4$ M$^{-1}$ cm$^{-1}$) located at 450 – 470 nm and ca. 290 – 330 nm, respectively. In **2A-Ru-P$^i$Pr$_2$Me**, the extinction coefficients are roughly doubled, due to the presence of two identical chromophores of type **1A-Ru-P$^i$Pr$_2$Me** within the molecule. Quantum chemical calculations on the full model of complex **1A-Ru-P$^i$Pr$_2$Me** [55] assign the underlying excitations to transitions between the delocalized HOMO and orbitals LUMO or LUMO+4, which are both localized on the anthrylene linker (for details to the calculations and a comparison between experimental and TD-DFT computed spectra, the corresponding electron density difference maps, as well as the results of Mulliken and NBO analyses, see Figures S46 – S51 and Tables S6 – S11 of the Supporting Information). The HOMO extends over the entire π-conjugated pathway, with equal contributions from the {Ru(CO)Cl(P$^i$Pr$_2$Me)$_2$} entities (51 %) and the 1,

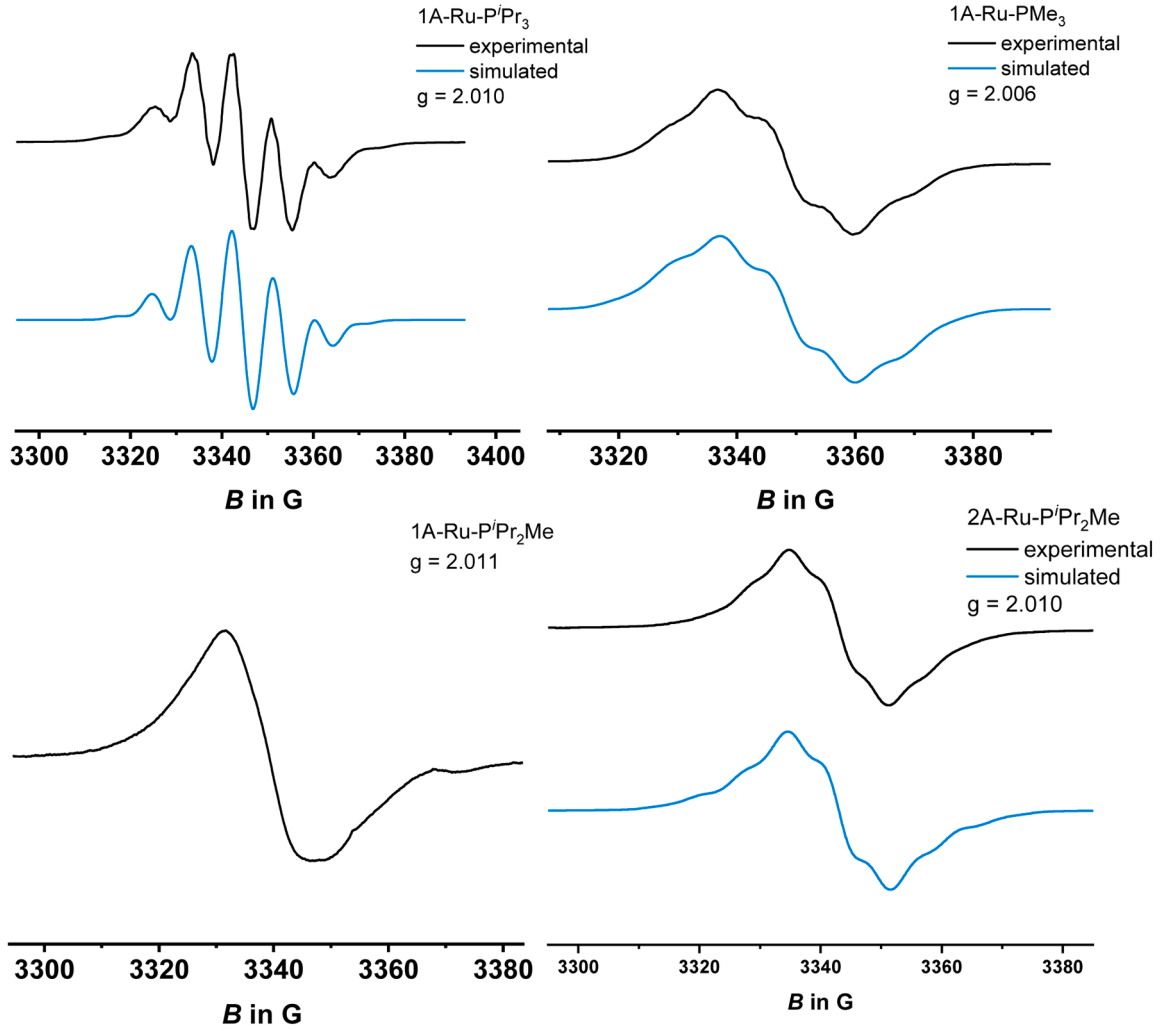


**Fig. 6.** Experimental (black) and simulated (blue) EPR spectra of **1A-Ru-P$^i$Pr$_3^{\bullet+}$** (top left), **1A-Ru-PMe$_3^{\bullet+}$** (top right), **1A-Ru-P$^i$Pr$_2$Me$^{\bullet+}$** (bottom left), and **2A-Ru-P$^i$Pr$_2$Me$^{\bullet\bullet 2+}$** (bottom right).

4-divinylanthrylene linker (49 %), while the LUMO and LUMO+4 are entirely bridge-based. Both transitions assume therefore mixed anthrylene intraligand and metal-to-anthrylene ligand charge-transfer character (see Table S6 and Figure S48 of the Supporting Information). Extended π-conjugation and enhanced charge-transfer contributions shift these bands to lower energy as compared to di- or tetraalkoxy-substituted anthracenes [91], protected dialkyne **LA-(ATMS)$_2$** (see Table 4 and Figure S42 of the Supporting Information), and other diethynylanthracenes [92]. Similar effects were observed on conversion of the latter dialkynes into gold acetylide complexes [92] or the 9,10-diethynylanthrylene-bridged diruthenium complex shown in Fig. 3 [84].

As expected, stepwise oxidation of the complexes gives rise to distinct changes in the electronic spectra. The results for **1A-Ru-P$^i$Pr$_3$** are shown in Fig. 7. Figures S43 and S44 provide the results for SEC experiments of complexes **1A-Ru-P$^i$Pr$_2$Me** and **2A-Ru-P$^i$Pr$_2$Me**, while Figure S45 compares the spectra of the neutral complexes and their mono- and dioxidized forms. For **1A-Ru-PMe$_3^{+/2+}$**, chemical oxidation provided superior results over the SEC approach, whereas all attempts to access one- or two-electron oxidized **1A-Ru-PPh$_3$** by either method proved futile owing to rapid decomposition. UV/Vis/NIR spectra of the radical cations and of dication **2A-Ru-P$^i$Pr$_2$Me$^{2+}$** are characterized by two absorption features, namely a Gaussian-shaped band at ca. 1000 to 1100 nm and a broad, richly structured band with separate peaks at 740 – 780 nm and 835 – 885 nm. The latter two features are characteristic of an anthracenyl radical cation ($\lambda_{max}$ = 652 and 709 nm) [93], but are expectedly red-shifted in the present systems due to extended π-conjugation. This is also substantiated by TD-DFT calculations. According to the contour diagrams of the involved MOs and the EDDM plots in Fig. 8, both bands originate from combined HOMO-LUMO transitions within the α and β manifolds and can therefore be classified as anthracene-centered excitations augmented by charge transfer from the metal ions to the bridge, similar to radical cations of the 9,10-diethynylanthrylene-bridged diruthenium complex in Fig. 3 [84] or 9,10-diethynylanthrylene-bridged bis(diarylamines) [94,95]. The narrow, Gaussian-shaped appearance of the NIR band is also a token of the strong involvement of the anthrylene linker to the oxidation [94–98]. The computed, rather balanced and symmetric charge density loss from the {Ru} complex entities of 0.32 $e^-$ each and the linker (0.36 $e^-$) complies with a completely delocalized electronic ground state of the radical cations.

On further oxidation, the NIR absorption vanishes, while the band at higher energy intensifies and shifts blue, to 600 – 635 nm. Again, clean isosbestic points were observed for **1A-Ru-P$^i$Pr$_3$**, **1A-Ru-P$^i$Pr$_2$Me**, and **2A-Ru-P$^i$Pr$_2$Me** (Fig. 7 and Figures S43 and S44 of the Supporting Information). Moreover, spectra taken from samples of **1A-Ru-PMe$_3^{2+}$** generated by chemical oxidation with acetylferrocenium hexafluoroantimonate ($E^{0/+}_{1/2}$ = 0.27 V) [85] match those from SEC experiments and the results of Liu and coworkers [21]. TD-DFT computed spectra of the singlet state, which is predicted to be energetically preferred by 4.4 kJ/mol, reproduce the experimental spectra of **1A-Ru-P$^i$Pr$_2$Me$^{2+}$** significantly better than those for the higher-lying triplet state (see Figures S50 and S51 of the Supporting Information). The prominent absorption band originates mainly from the HOMO-1 and HOMO-3 → LUMO transitions with a concomitant shift of electron density from the metal ions and the π-donor chlorido ligands to a metal-bridge delocalized acceptor orbital, which resembles the HOMO of the neutral complex closely.

We note that our quantum chemical modelling only captured the delocalized ground-state structure of radical cation **1A-Ru-P$^i$Pr$_2$Me$^{\bullet+}$**, where the vinyl ruthenium moieties are nearly coplanar with the 1,4-divinylanthrylene linker as is evident from torsion angles Ru-C=C-C$_{Anthracenylene}$ of 178.3° and 178.4° Our experimental IR and EPR data on specifically the **1A-Ru-P$^i$Pr$_2$Me$^{\bullet+}$** radical cation have however provided some hints as to a coexisting valence-localized isomer, where one or both alkenyl ruthenium moieties are presumably rotated out of the bridge plane, thereby decoupling it from the remaining chromophore. The UV/Vis/NIR spectrum of **1A-Ru-P$^i$Pr$_2$Me$^{\bullet+}$** further supports this view, as the characteristic NIR and the structured Vis bands of the delocalized, open-shell chromophore are observed with significantly attenuated extinction coefficients, side by side with the stronger band characteristic of the dicationic forms with a full positive charge on every {Ru}-CH=CH-anthrylene subunit (see Figure S43 of the Supporting Information). All our attempts to model such a valence-localized isomer however failed to converge to a stable, second minimum structure.

## 4. Summary and conclusion

In summary, our present studies on **1A-Ru-P$^i$Pr$_3$**, **1A-Ru-PPh$_3$**, **1A-Ru-PMe$_3$**, **1A-Ru-P$^i$Pr$_2$Me**, and the derived metallamacrocycle **2A-Ru-P$^i$Pr$_2$Me** address the question, to what extent and how phosphine coligands influence the stereoelectronic and (electro)chemical properties of 1,4-divinylanthrylene-bridged diruthenium complexes and the stabilities of their associated oxidized forms. First differences are already seen in voltammetric measurements. Although the ruthenium ions in complexes **1A-Ru-P$^i$Pr$_3$** and **1A-Ru-P$^i$Pr$_2$Me** achieve only a 16 valence electron count, they are easier to oxidize than **1A-Ru-PMe$_3$** with coordinatively saturated, six-coordinated ruthenium entities. Moreover, **1A-Ru-P$^i$Pr$_3$** and **2A-Ru-P$^i$Pr$_2$Me** exhibit two consecutive, fully reversible two- / four-electron oxidations. **1A-Ru-P$^i$Pr$_2$Me**, **1A-Ru-PMe$_3$**, and, in

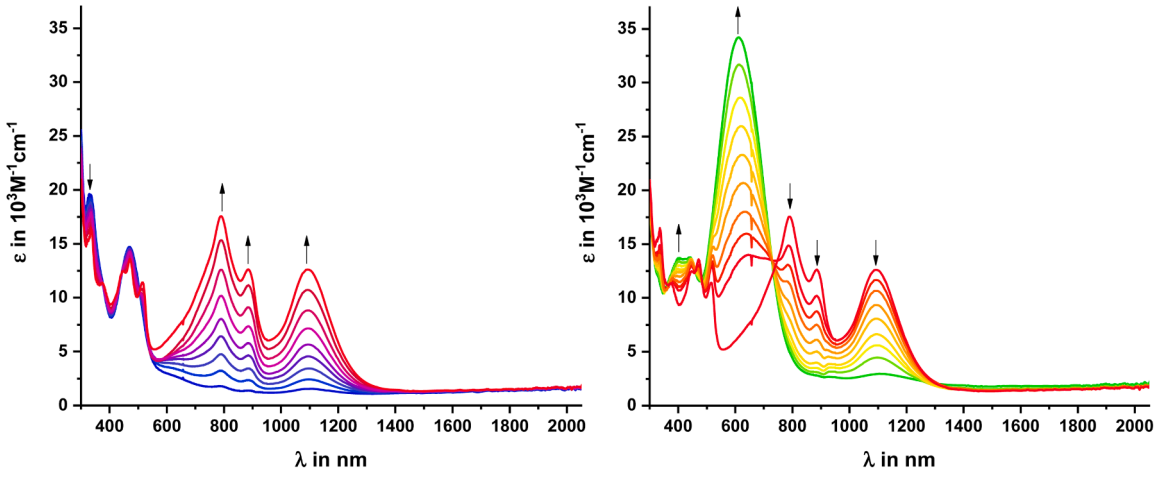


**Fig. 7.** Changes of UV/Vis/NIR spectra during electrochemical oxidation of **1A-Ru-P$^i$Pr$_3$** to the monocation (left) and further oxidation to its dication (right) in 0.2 M 1,2-$C_2H_4Cl_2$ / $^nBu_4N^+PF_6^-$ at r.t.

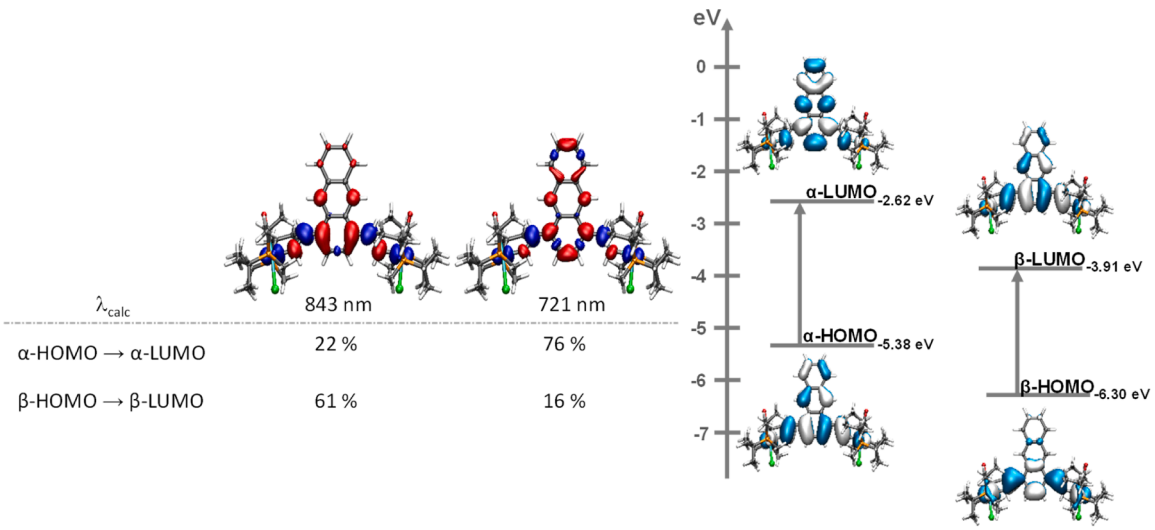


**Fig. 8.** Contour diagrams of the acceptor and donor molecular orbitals involved in the electronic transitions of **1A-Ru-P$^{i}$Pr$_2$Me$^{\bullet+}$** with the corresponding electron density difference maps (EDDMs). Blue color indicates an electron density decrease, red color an electron density increase.

particular, **1A-Ru-PPh$_3$** show inferior performance due to chemical and/or kinetic issues. We could nevertheless generate and investigate the one- and two-electron oxidized cations of all complexes except for **1A-Ru-PPh$_3$** by means of IR, UV/Vis/NIR and, in their open-shell, mixed-valent states, also by EPR spectroscopy. As shown by their IR and EPR spectra, the mixed-valent radical cations and dication **2A-Ru-P$^{i}$Pr$_2$Me$^{2+}$** have intrinsically delocalized electronic ground states with large, if not dominant, bridge contributions to the relevant redox orbital, i. e. the HOMO of their neutral forms and the β-LUMO of their radical cation. The ordering of redox potentials is also mirrored by variations in the energy of the CO stretching vibrations of the ruthenium-bonded carbonyl ligands, which is a faithful reporter of the electron density at the metal ions. Radical cations with delocalized electronic structures and the dications have identical CO band positions, meaning that bridge and metal contributions to the redox processes vary slightly between the individual congeners, which results in uniform electron density distributions. A peculiar behavior is, however, noted for **1A-Ru-P$^{i}$Pr$_2$Me$^{\bullet+}$**, for which our spectroscopic data suggest the presence of coexisiting valence-delocalized and valence-trapped forms. Electronic decoupling is likely triggered by the twisting of one vinyl-ruthenium moiety out of the plane of the anthrylene linker.

## CRediT authorship contribution statement

**Franciska S. Gogesch:** Writing – review & editing, Writing – original draft, Visualization, Investigation, Data curation. **Jonas Rendler:** Investigation. **Michael Linseis:** Methodology, Investigation, Data curation. **Laura Senft:** Methodology, Investigation. **Ivana Ivanović-Burmazović:** Methodology, Funding acquisition. **Rainer F. Winter:** Writing – review & editing, Writing – original draft, Project administration, Funding acquisition, Conceptualization.

## Declaration of competing interest

The authors declare that they have no known conflicting financial interests or personal relationships that could have appeared to influence the work reported in this paper.

## Data availability

Data will be made available on request.

## Acknowledgements

We gratefully acknowledge financial support of this work by the German Research Foundation (Deutsche Forschungsgemeinschaft, DFG) through grant Wi1262/17–1. The authors also acknowledge support by the state of Baden-Württemberg through bwHPC and the German Research Foundation (Deutsche Forschungsgemeinschaft, DFG) for granting us access to the supercomputing facilities of the JUSTUS2 supercomputing facilities (grant number INST 40/575–1 FUGG). This work also employed the NMR Core Facility of the University of Konstanz. The authors also acknowledge financial support by the open-access funds of the Universität Konstanz.

## Supplementary materials

Supplementary material associated with this article can be found, in the online version, at doi:10.1016/j.jorganchem.2024.123185.

## References

[1] J. Maurer, B. Sarkar, B. Schwederski, W. Kaim, R.F. Winter, S. Záliš, Divinylphenylene-bridged diruthenium complexes bearing Ru(CO)Cl(P$^{i}$Pr$_3$)$_2$ entities, Organometallics 25 (15) (2006) 3701–3712, https://doi.org/10.1021/om0602660.

[2] S. Scheerer, N. Rotthowe, O.S. Abdel-Rahman, X. He, S. Rigaut, H. Kvapilová, S. Záliš, R.F. Winter, Vinyl ruthenium-modified biphenyl and 2,2′-bipyridines, Inorg. Chem. 54 (7) (2015) 3387–3402, https://doi.org/10.1021/ic503075e.

[3] U. Pfaff, A. Hildebrandt, M. Korb, S. Oßwald, M. Linseis, K. Schreiter, S. Spange, R. F. Winter, H. Lang, Electronically strongly coupled divinylheterocyclic-bridged diruthenium complexes, Chem. Eur. J. 22 (2) (2016) 783–801, https://doi.org/10.1002/chem.201503687.

[4] P. Mücke, M. Zabel, R. Edge, D. Collison, S. Clément, S. Záliš, R.F. Winter, Electron delocalization in vinyl ruthenium substituted cyclophanes: assessment of the through-space and the through-bond pathways, J. Organomet. Chem. 696 (20) (2011) 3186–3197, https://doi.org/10.1016/j.jorganchem.2011.06.028.

[5] M. Linseis, S. Záliš, M. Zabel, R.F. Winter, Ruthenium stilbenyl and diruthenium distyrylethene complexes: aspects of electron delocalization and electrocatalyzed isomerization of the Z-Isomer, J. Am. Chem. Soc. 134 (40) (2012) 16671–16692, https://doi.org/10.1021/ja3059606.

[6] E. Anger, M. Srebro, N. Vanthuyne, L. Toupet, S. Rigaut, C. Roussel, J. Autschbach, J. Crassous, R. Réau, Ruthenium-vinylhelicenes: remote metal-based enhancement and redox switching of the chiroptical properties of a helicene core, J. Am. Chem. Soc. 134 (38) (2012) 15628–15631, https://doi.org/10.1021/ja304424t.

[7] G. Jia, W.F. Wu, R.C. Yeung, H.P. Xia, Dimeric and polymeric ruthenium complexes with Ru-vinyl linkages, J. Organomet. Chem. 539 (1–2) (1997) 53–59, https://doi.org/10.1016/S0022-328X(97)00080-6.

[8] S.K. Seetharaman, M.-C. Chung, U. Englich, K. Ruhlandt-Senge, M.B. Sponsler, Temperature-dependent coordination of phosphine to five-coordinate alkenylruthenium complexes, Inorg. Chem. 46 (2) (2007) 561–567, https://doi.org/10.1021/ic061389f.

[9] B. Gómez-Lor, A. Santos, M. Ruiz, A.M. Echavarren, Ruthenium-capping of Di- and Tetraethynylbiphenyls, Eur. J. Inorg. Chem. (9) (2001) 2305–2310, https://doi.org/10.1002/1099-0682(200109)2001:9<2305:AID−EJIC2305>3.0.CO;2-T.

[10] J. Maurer, M. Linseis, B. Sarkar, B. Schwederski, M. Niemeyer, W. Kaim, S. Zalis, C. Anson, M. Zabel, R.F. Winter, Ruthenium complexes with vinyl, styryl, and vinylpyrenyl ligands: a case of non-innocence in organometallic chemistry, J. Am. Chem. Soc. 130 (1) (2008) 259–268, https://doi.org/10.1021/ja075547t.

[11] X.H. Wu, S. Jin, J.H. Liang, Z.Y. Li, G.-A. Yu, S.H. Liu, Synthesis, characterization, and substituent effects of binuclear ruthenium vinyl complexes [RuCl(CO)$(PMe_3)_3]_2$(μ-CH=CH−Ar−CH=CH), Organometallics 28 (8) (2009) 2450–2459, https://doi.org/10.1021/om900018y.

[12] W.Y. Man, J.-L. Xia, N.J. Brown, J.D. Farmer, D.S. Yufit, J.A.K. Howard, S.H. Liu, P. J. Low, Spectroscopic and computational studies of the ligand redox non-innocence in mono- and binuclear ruthenium vinyl complexes, Organometallics 30 (7) (2011) 1852–1858, https://doi.org/10.1021/om1010534.

[13] D.-D. Kong, L.-S. Xue, R. Jang, B. Liu, X.-G. Meng, S. Jin, Y.-P. Ou, X. Hao, S.-H. Liu, Conformational tuning of the intramolecular electronic coupling in molecular-wire biruthenium complexes bridged by biphenyl derivatives, Chem. Eur. J. 21 (27) (2015) 9895–9904, https://doi.org/10.1002/chem.201500509.

[14] J. Zhang, C.-F. Sun, X.-H. Wu, M.-X. Zhang, J. Yin, G.-A. Yu, S.H. Liu, Bimetallic ruthenium vinyl complexes bridged by electronic substituent phenylenes: spectroelectrochemical and computational studies, Int. J. Electrochem. Sci. 11 (2016) 7875–7889, https://doi.org/10.20964/2016.09.34.

[15] W.-X. Liu, F. Yan, S.-L. Qian, J.-Y. Ye, X. Liu, M.-X. Yu, X.-H. Wu, M.-L. Le, Z.-Y. Zhou, S.-H. Liu, P.J. Low, S. Jin, Electronic structures of divinylchalcogenophene-bridged biruthenium complexes: exploring trends from O to Te, Eur. J. Inorg. Chem. (43) (2017) 5015–5026, https://doi.org/10.1002/ejic.201701036.

[16] F. Li, J. Cheng, X. Chai, S. Jin, X. Wu, G.-A. Yu, S.H. Liu, G.Z. Chen, Synthesis, characterization, and electrochemical properties of diruthenium complexes bridged by anthraquinones, Organometallics 30 (7) (2011) 1830–1837, https://doi.org/10.1021/om100932u.

[17] Y.-P. Ou, C. Jiang, Di Wu, J. Xia, J. Yin, S. Jin, G.-A. Yu, S.H. Liu, Synthesis, characterization, and properties of anthracene-bridged bimetallic ruthenium vinyl complexes [RuCl(CO)$(PMe_3)_3]_2$(μ-CH=CH-anthracene-CH=CH), Organometallics 30 (21) (2011) 5763–5770, https://doi.org/10.1021/om200622q.

[18] Y.-P. Ou, J. Zhang, M. Xu, J. Xia, F. Hartl, J. Yin, G.-A. Yu, S.H. Liu, Bridge-localized HOMO-binding character of divinylanthracene-bridged dinuclear ruthenium carbonyl complexes: spectroscopic, spectroelectrochemical, and computational studies, Chem. Asian J. 9 (4) (2014) 1152–1160, https://doi.org/10.1002/asia.201301544.

[19] P. Yuan, X.-H. Wu, G.-A. Yu, D. Du, S.H. Liu, Synthesis and characterization of bimetallic ruthenium complexes connected through linear $(CH)_{14}$ chain, J. Organomet. Chem. 692 (16) (2007) 3588–3592, https://doi.org/10.1016/j.jorganchem.2007.04.040.

[20] S.H. Liu, Y. Chen, K.L. Wan, T.B. Wen, Z. Zhou, M.F. Lo, I.D. Williams, G. Jia, Synthesis and characterization of linear $(CH)_8$-bridged bimetallic ruthenium complexes, Organometallics 21 (23) (2002) 4984–4992, https://doi.org/10.1021/om020442e.

[21] Y.-P. Ou, J. Zhang, Y. Hu, J. Yin, C. Chi, S.H. Liu, Oxidized divinyl oligoacene-bridged diruthenium complexes: bridged localized radical characters and reduced aromaticity in bridge cores, Dalton Trans. 49 (46) (2020) 16877–16886, https://doi.org/10.1039/D0DT02883E.

[22] H.P. Xia, R.C.Y. Yeung, G. Jia, Synthesis and characterization of bimetallic ruthenium complexes bridged with linear $C_4H_4$ and $C_6H_4O_2$ ligands, Organometallics 22 (22) (1998) 4762–4768, https://doi.org/10.1021/om9804935.

[23] E. Wuttke, Y.-M. Hervault, W. Polit, M. Linseis, P. Erler, S. Rigaut, R.F. Winter, Divinylphenylene- and ethynylvinylphenylene-bridged mono-, di-, and triruthenium complexes for covalent binding to gold electrodes, Organometallics 33 (18) (2014) 4672–4686, https://doi.org/10.1021/om400642j.

[24] F. Pevny, R.F. Winter, B. Sarkar, S. Záliš, How to elucidate and control the redox sequence in vinylbenzoate and vinylpyridine bridged diruthenium complexes, Dalton. Trans. 39 (34) (2010) 8000–8011, https://doi.org/10.1039/C0DT00164C.

[25] C. Hassenrück, M. Azarkh, M. Drescher, M. Linseis, S. Demeshko, F. Meyer, R. F. Winter, Redox isomeric ferrocenyl styrylruthenium radical cations with diphenyl-substituted β-ketoenolato ligands, Organometallics 39 (1) (2020) 153–164, https://doi.org/10.1021/acs.organomet.9b00714.

[26] C. Hassenrück, A. Mang, R.F. Winter, Mixed-valent ruthenocene-vinylruthenium conjugates: valence delocalization despite chemically different redox sites, Inorg. Chem. 58 (4) (2019) 2695–2707, https://doi.org/10.1021/acs.inorgchem.8b03253.

[27] R. Das, M. Linseis, S.M. Schupp, L. Schmidt-Mende, R.F. Winter, Electron-rich diruthenium complexes with π-extended alkenyl ligands and their $F_4$TCNQ charge-transfer salts, Chem. Eur. J. 28 (23) (2022) e202104403, https://doi.org/10.1002/chem.202104403.

[28] S.H. Liu, H. Xia, T.B. Wen, Z. Zhou, G. Jia, Synthesis and characterization of bimetallic ruthenium complexes with $(CH)_6$ and related bridges, Organometallics 22 (4) (2003) 737–743, https://doi.org/10.1021/om0207663.

[29] X.-H. Wu, J.H. Liang, J.-L. Xia, S. Jin, G.-A. Yu, S.H. Liu, Bimetallic ruthenium complexes: synthesis, characterization, and the effect of appending long carbon chains to their bridges, Organometallics 29 (5) (2010) 1150–1156, https://doi.org/10.1021/om901025q.

[30] P. Yuan, S.H. Liu, W. Xiong, J. Yin, G.-A. Yu, H.Y. Sung, I.D. Williams, G. Jia, Synthesis and characterization of $(CHCH)_3$-bridged heterobimetallic ferrocene−ruthenium complexes, Organometallics 24 (7) (2005) 1452–1457, https://doi.org/10.1021/om0490637.

[31] Y. Lin, J. Yuan, M. Hu, J. Cheng, J. Yin, S. Jin, S.H. Liu, Syntheses and properties of binuclear ruthenium vinyl complexes with dithienylethene units as multifunction switches, Organometallics 28 (22) (2009) 6402–6409, https://doi.org/10.1021/om900396b.

[32] J. Zhang, Y. Ou, M. Xu, C. Sun, J. Yin, G.-A. Yu, S.H. Liu, Synthesis and characterization of dibenzoheterocycle-bridged dinuclear ruthenium alkynyl and vinyl complexes, Eur. J. Inorg. Chem. (18) (2014) 2941–2951, https://doi.org/10.1002/ejic.201402106.

[33] H. Werner, M.A. Esteruelas, H. Otto, Insertion reactions of the 16-electron complexesMHCl(CO)$[P(CHMe_2)_3]_2$ (M = Ru, Os) with alkynes. The X-ray crystal structure of [(*E*)-PhCH=CHOs(Cl)$[P(CHMe_2)_3]_2$, Organometallics 5 (11) (1986) 2295–2299, https://doi.org/10.1021/om00142a019.

[34] S. Jung, K. Ilg, C.D. Brandt, J. Wolf, H. Werner, A series of vinylidene-, Vinyl-, Carbene- and Carbyneruthenium(II) complexes with $[Ru(PCy_3)_2]$ and $[Ru(P^iPr_3)_2]$ as molecular building blocks, Eur. J. Inorg. Chem. (3) (2004) 469–480, https://doi.org/10.1002/ejic.200300496.

[35] H. Werner, W. Stüer, B. Weberndörfer, J. Wolf, Hydrido(carbonyl) and Hydrido (carbene) complexes of ruthenium, Chem. Ber. (10) (1999) 1707–1713, https://doi.org/10.1002/(SICI)1099-0682(199910)1999:10<1707:AID−EJIC1707>3.0.CO;2-Y.

[36] H. Werner, U. Meyer, K. Peters, H.G. Schnering, Fünf- und sechsfach koordinierte Vinylruthenium- und -osmium-Komplexe durch Alkin-Insertion in Hydridometall-Vorstufen, Chem. Ber. 122 (11) (1989) 2097–2107, https://doi.org/10.1002/cber.19891221109.

[37] M.A. Esteruelas, F.J. Lahoz, E. Onate, L.A. Oro, B. Zeier, Reactions of RuHCl(CO)$(P^iPr_3)_2$ with Alkyn-1-ols: synthesis of Ruthenium(II) Hydroxyvinyl and Vinylcarbene complexes, Organometallics 13 (11) (1994) 4258–4265, https://doi.org/10.1021/om00023a031.

[38] M.L. Buil, M.A. Esteruelas, Synthesis and characterization of ruthenium−osmium complexes containing μ-Bisalkenyl, μ-Alkenylvinylidene, and μ-Alkenylcarbene bridge ligands, Organometallics 18 (9) (1999) 1798–1800, https://doi.org/10.1021/om9810192.

[39] A.V. Marchenko, H. Gérard, O. Eisenstein, K.G. Caulton, A comparative study of olefin or acetylene insertion into Ru–H or Os–H of MHCl(CO)$(phosphine)_2$, New J. Chem. 25 (11) (2001) 1382–1388, https://doi.org/10.1039/B103113A.

[40] A.V. Marchenko, J.C. Huffman, P. Valerga, M.J. Tenorio, M.C. Puerta, K. G. Caulton, Effect of Lewis acidity on the synthesis of RuHCl(CO)$(phosphine)_2$: subtle influence of steric and electronic effects among $P^iPr_3$, $P^iPr_2(3,5\text{-}(CF_3)_2C_6H_3)$, and $P^iPr_2Me$, Inorg. Chem. 40 (25) (2001) 6444–6450, https://doi.org/10.1021/ic000500t.

[41] S. Jung, C.D. Brandt, J. Wolf, H. Werner, Vinyl and carbene ruthenium(II) complexes from hydridoruthenium(II) precursors, Dalton Trans. (3) (2004) 375–383, https://doi.org/10.1039/B314425A.

[42] X. Wu, T. Weng, S. Jin, J. Liang, R. Guo, G.-A. Yu, S.H. Liu, Synthesis, characterization, and substituent effects of mononuclear ruthenium complexes [RuCl(CO)$(PMe_3)_3$(CHCH-$C_6H_4$-R-p)] (R=H, $CH_3$, $OCH_3$, $NO_2$, $NH_2$, $NMe_2$), J. Organomet. Chem. 694 (12) (2009) 1877–1883, https://doi.org/10.1016/j.jorganchem.2009.01.024.

[43] O.S. Abdel-Rahman, J. Maurer, S. Záliš, R.F. Winter, Ruthenium styryl complexes with ligands derived from 2-Hydroxy- and 2-Mercaptopyridine and 2-Hydroxy- and 2-Mercaptoquinoline, Organometallics 34 (14) (2015) 3611–3628, https://doi.org/10.1021/acs.organomet.5b00401.

[44] E. Wuttke, D. Fink, P. Anders, A.-L.Maria Hoyt, W. Polit, M. Linseis, R.F. Winter, Homo- and heterobimetallic 1,4-divinylphenylene- and naphthalene-1,8-divinyl-bridged diruthenium, diosmium and ruthenium osmium complexes, J. Organomet. Chem. 821 (15) (2016) 4–18, https://doi.org/10.1016/j.jorganchem.2016.02.031.

[45] P. Anders, M. Rapp, M. Linseis, R. Winter, Tetraruthenium metallamacrocycles with potentially coordinating appended functionalities, Inorganics 6 (3) (2018) 73–94, https://doi.org/10.3390/inorganics6030073.

[46] S. Scheerer, M. Linseis, E. Wuttke, S. Weickert, M. Drescher, O. Tröppner, I. Ivanović-Burmazović, A. Irmler, F. Pauly, R.F. Winter, Redox-active tetraruthenium macrocycles built from 1,4-Divinylphenylene-bridged diruthenium complexes, Chem. Eur. J. 22 (28) (2016) 9574–9590, https://doi.org/10.1002/chem.201601384.

[47] D. Fink, A. Staiger, N. Orth, M. Linseis, I. Ivanović-Burmazović, R.F. Winter, Redox-induced hydrogen bond reorientation mimicking electronic coupling in mixed-valent diruthenium and macrocyclic tetraruthenium complexes, Inorg. Chem. 59 (22) (2020) 16703–16715, https://doi.org/10.1021/acs.inorgchem.0c02695.

[48] Y. Li Tian, Y.M. Liu, G.-X. Tian, X.H. Wu, Z. Li, J.-F. Kou, Y.-P. Ou, S.H. Liu, W.-F. Fu, Bimetallic ruthenium complexes bridged by divinylphenylene bearing oligo (ethylene glycol)methylether: synthesis, (spectro)electrochemistry and the lithium cation effect, Dalton Trans 43 (10) (2014) 4093–4101, https://doi.org/10.1039/c3dt52677a.

[49] J.B.G. Gluyas, S. Gückel, M. Kaupp, P.J. Low, Rational control of conformational distributions and mixed-valence characteristics in diruthenium complexes, Chem. Eur. J. 22 (45) (2016) 16138–16146, https://doi.org/10.1002/chem.201603236.

[50] M. Gantenbein, X. Li, S. Sangtarash, J. Bai, G. Olsen, A. Alqorashi, W. Hong, C. J. Lambert, M.R. Bryce, Exploring antiaromaticity in single-molecule junctions formed from biphenylene derivatives, Nanoscale 11 (43) (2019) 20659–20666, https://doi.org/10.1039/c9nr05375a.

[51] M.A. Esteruelas, H. Werner, Five- and six-coordinate hydrido(carbonyl)-ruthenium (II) and -osmium(II) complexes containing triisopropylphosphine as ligand, J. Organomet. Chem. 303 (2) (1986) 221–231, https://doi.org/10.1016/0022-328X(86)80134-6.

[52] D.B. Eremin, E.A. Denisova, A.Yu Kostyukovich, J. Martens, G. Berden, J. Oomens, V.N. Khrustalev, V.M. Chernyshev, V.P. Ananikov, Ionic Pd/NHC catalytic system enables recoverable homogeneous catalysis: mechanistic study and application in the Mizoroki-Heck reaction, Chem. Eur. J. 25 (72) (2019) 16564–16572, https://doi.org/10.1002/chem.201903221.

[53] M. Krejčik, M. Daněk, F. Hartl, Simple construction of an infrared optically transparent thin-layer electrochemical cell: applications to the redox reactions of ferrocene, $Mn_2(CO)_{10}$ and $Mn(CO)_3$(3,5-di-t-butyl-catecholate)−, J. Electroanal. Chem. 317 (1–2) (1991) 179–187, https://doi.org/10.1016/0022-0728(91)85012-E.

[54] S. Stoll, A. Schweiger, EasySpin, a comprehensive software package for spectral simulation and analysis in EPR, J. Magn. Reson. 178 (1) (2006) 42–55, https://doi.org/10.1016/j.jmr.2005.08.013.

[55] M.J. Frisch, G.W. Trucks, H.B. Schlegel, G.E. Scuseria, M.A. Robb, J.R. Cheeseman, G. Scalmani, V. Barone, G.A. Petersson, H. Nakatsuji, X. Li, M. Caricato, A. Marenich, J. Bloino, B.G. Janesko, R. Gomperts, B. Mennucci, H.P. Hratchian, J. V. Ortiz, A.F. Izmaylov, J.L. Sonnenberg, D. Williams-Young, F. Ding, F. Lipparini, F. Egidi, J. Goings, B. Peng, A. Petrone, T. Henderson, D. Ranasinghe, V. G. Zakrzewski, J. Gao, N. Rega, G. Zheng, W. Liang, M. Hada, M. Ehara, K. Toyota, R. Fukuda, J. Hasegawa, M. Ishida, T. Nakajima, Y. Honda, O. Kitao, H. Nakai, T. Vreven, K. Throssell, J.J.A. Montgomery, J.E. Peralta, F. Ogliaro, M. Bearpark, J. J. Heyd, E. Brothers, K.N. Kudin, V.N. Staroverov, T. Keith, R. Kobayashi, J. Normand, K. Raghavachari, A. Rendell, J.C. Burant, S.S. Iyengar, J. Tomasi, M. Cossi, J.M. Millam, M. Klene, C. Adamo, R. Cammi, J.W. Ochterski, R.L. Martin, K. Morokuma, O. Farkas, J.B. Foresman, D.J. Fox, GAUSSIAN09, Gaussian 09, Revision D.01, Gaussian, Inc, Wallingford, CT, 2009.

[56] S. Grimme, J. Antony, S. Ehrlich, H. Krieg, A consistent and accurate ab initio parametrization of density functional dispersion correction (DFT-D) for the 94 elements H-Pu, J. Chem. Phys. 132 (15) (2010) 154104, https://doi.org/10.1063/1.3382344.

[57] M. Cossi, N. Rega, G. Scalmani, V. Barone, Energies, structures, and electronic properties of molecules in solution with the C-PCM solvation model, J. Comput. Chem. 24 (6) (2003) 669–681, https://doi.org/10.1002/jcc.10189.

[58] P.C. Hariharan, J.A. Pople, The influence of polarization functions on molecular orbital hydrogenation energies, Theoret. Chim. Acta 28 (3) (1973) 213–222, https://doi.org/10.1007/BF00533485.

[59] J.P. Perdew, K. Burke, M. Ernzerhof, Generalized gradient approximation made simple, Phys. Rev. Lett. 77 (18) (1996) 3865–3868, https://doi.org/10.1103/PhysRevLett.77.3865.

[60] C. Adamo, V. Barone, Toward reliable density functional methods without adjustable parameters: the PBE0 model, J. Chem. Phys. 110 (13) (1999) 6158–6170, https://doi.org/10.1063/1.478522.

[61] N.M. O'Boyle, A.L. Tenderholt, K.M. Langner, cclib: a library for package-independent computational chemistry algorithms, J. Comput. Chem. 29 (5) (2008) 839–845, https://doi.org/10.1002/jcc.20823.

[62] M.D. Hanwell, D.E. Curtis, D.C. Lonie, T. Vandermeersch, E. Zurek, G.R. Hutchison, Avogadro: an advanced semantic chemical editor, visualization, and analysis platform, J. Cheminf. 17 (4) (2012) 1–17, https://doi.org/10.1186/1758-2946-4-17.

[63] O. Tange, Gnu parallel-the command-line power tool, USENIX Magaz 36 (36) (2011) 42–47, https://doi.org/10.5281/zenodo.16303.

[64] W. Humphrey, A. Dalke, K. Schulten, VMD: visual molecular dynamics, J. Mol. Graphics 14 (1) (1996) 33–38, https://doi.org/10.1016/0263-7855(96)00018-5.

[65] O.V. Dolomanov, L.J. Bourhis, R.J. Gildea, J.A.K. Howard, H. Puschmann, OLEX2 a complete structure solution, refinement and analysis program, J. Appl. Cryst. 42 (2) (2009) 339–341, https://doi.org/10.1107/S0021889808042726.

[66] G.M. Sheldrick, Crystal structure refinement with SHELXL, Acta Cryst. C 71 (1) (2015) 3–8, https://doi.org/10.1107/S2053229614024218.

[67] L.J. Farrugia, WinGX and ORTEP for Windows an update, J. Appl. Cryst. 45 (4) (2012) 849–854, https://doi.org/10.1107/S0021889812029111.

[68] A.L. Spek, Single-crystal structure validation with the program PLATON, J. Appl. Cryst. 36 (1) (2003) 7–13, https://doi.org/10.1107/S0021889802022112.

[69] C.F. Macrae, I. Sovago, S.J. Cottrell, P.T.A. Galek, P. McCabe, E. Pidcock, M. Platings, G.P. Shields, J.S. Stevens, M. Towler, P.A. Wood, Mercury 4.0: from visualization to analysis, design and prediction, J. Appl. Cryst. 53 (1) (2020) 226–235, https://doi.org/10.1107/S1600576719014092.

[70] D. Fink, N. Orth, V. Ebel, F.S. Gogesch, A. Staiger, M. Linseis, I. Ivanović-Burmazović, R.F. Winter, Self-assembled redox-active tetraruthenium macrocycles with large intracyclic cavities, Organometallics 39 (10) (2020) 1861–1880, https://doi.org/10.1021/acs.organomet.0c00116.

[71] D. Fink, M. Linseis, R.F. Winter, Constitutional isomers of macrocyclic tetraruthenium complexes with vastly different spectroscopic and electrochemical properties, Organometallics 37 (12) (2018) 1817–1820, https://doi.org/10.1021/acs.organomet.8b00057.

[72] S.H. Liu, Q.Y. Hu, P. Xue, T.B. Wen, I.D. Williams, G. Jia, Synthesis and characterization of $C_{10}H_{10}$-bridged bimetallic ruthenium complexes, Organometallics 24 (4) (2005) 769–772, https://doi.org/10.1021/om0493659.

[73] X.H. Wu, J.H. Liang, J.L. Xia, J. Yin, S. Jin, G.-A. Yu, S.H. Liu, Synthesis, characterization, and properties of binuclear ruthenium complexes with dendritic side chains on their bridges, Inorg. Chim. Acta 370 (1) (2011) 286–291, https://doi.org/10.1016/j.ica.2011.01.075.

[74] F. Barrière, N. Camire, W.E. Geiger, U.T. Mueller-Westerhoff, R. Sanders, Use of medium effects to tune the $\Delta E_{1/2}$ values of bimetallic and oligometallic compounds, J. Am. Chem. Soc. 124 (25) (2002) 7262–7263, https://doi.org/10.1021/ja020309d.

[75] F. Barrière, W.E. Geiger, Use of weakly coordinating anions to develop an integrated approach to the tuning of $\Delta E_{1/2}$ values by medium effects, J. Am. Chem. Soc. 128 (12) (2006) 3980–3989, https://doi.org/10.1021/ja058171x.

[76] D.R. Laws, D. Chong, K. Nash, A.L. Rheingold, W.E. Geiger, Cymantrene radical cation family: spectral and structural characterization of the half-sandwich analogues of ferrocenium ion, J. Am. Chem. Soc. 130 (30) (2008) 9859–9870, https://doi.org/10.1021/ja801930q.

[77] J.C. Swarts, A. Nafady, J.H. Roudebush, S. Trupia, W.E. Geiger, One-electron oxidation of ruthenocene: reactions of the ruthenocenium ion in gentle electrolyte media, Inorg. Chem. 48 (5) (2009) 2156–2165, https://doi.org/10.1021/ic802105b.

[78] N. Camire Ohrenberg, L.M. Paradee, R.J. DeWitte, D. Chong, W.E. Geiger, Spectra and synthetic-time-scale substitution reactions of electrochemically produced $[Cr(CO)_3(\eta^6\text{-arene})]^+$ complexes, Organometallics 29 (14) (2010) 3179–3186, https://doi.org/10.1021/om100318q.

[79] S. Scheerer, Von Divinylarylen- und Tetraoxolenverbrückten Diruthenium-Komplexen zu Metallamakrozyklen, Dissertation, Universität Konstanz, 2017.

[80] N. Rotthowe, J. Zwicker, R.F. Winter, Influence of quinoidal distortion on the electronic properties of oxidized divinylarylene-bridged diruthenium complexes, Organometallics 38 (14) (2019) 2782–2799, https://doi.org/10.1021/acs.organomet.9b00318.

[81] A.B.P. Lever, Electrochemical parametrization of metal complex redox potentials, using the Ruthenium(III)/Ruthenium(II) couple to generate a ligand electrochemical series, Inorg. Chem. 29 (6) (1990) 1271–1285, https://doi.org/10.1021/ic00331a030.

[82] C.A. Tolman, Steric effects of phosphorus ligands in organometallic chemistry and homogeneous catalysis, Chem. Rev. 77 (3) (1977) 313–348, https://doi.org/10.1021/cr60307a002.

[83] A.L. Fernandez, T.Y. Lee, C. Reyes, A. Prock, W.P. Giering, A thermodynamically based and definitive demonstration of the inadequacy of the ECW model for Phosphorus(III) Ligands, Organometallics 17 (15) (1998) 3169–3175, https://doi.org/10.1021/om980262y.

[84] M.A. Fox, B.Le Guennic, R.L. Roberts, D.A. Brue, D.S. Yufit, J.A.K. Howard, G. Manca, J.-F. Halet, F. Hartl, P.J. Low, Simultaneous bridge-localized and mixed-valence character in diruthenium radical cations featuring diethynylaromatic bridging ligands, J. Am. Chem. Soc. 133 (45) (2011) 18433–18446, https://doi.org/10.1021/ja207827m.

[85] N.G. Connelly, W.E. Geiger, Chemical redox agents for organometallic chemistry, Chem. Rev. 96 (2) (1996) 877–910, https://doi.org/10.1021/cr940053x.

[86] S. Marqués-González, M. Parthey, D.S. Yufit, J.A.K. Howard, M. Kaupp, P.J. Low, Combined spectroscopic and quantum chemical study of $[trans\text{-}Ru(C{\equiv}CC_6H_4R^1\text{-}4)_2(dppe)_2]^{n+}$ and $[trans\text{-}Ru(C{\equiv}CC_6H_4R^1\text{-}4)(C{\equiv}CC_6H_4R^2\text{-}4)(dppe)_2]^{n+}$ (n = 0, 1) complexes: interpretations beyond the lowest energy conformer paradigm, Organometallics 33 (18) (2014) 4947–4963, https://doi.org/10.1021/om500265s.

[87] M. Parthey, J.B.G. Gluyas, M.A. Fox, P.J. Low, M. Kaupp, Mixed-valence ruthenium complexes rotating through a conformational Robin-Day continuum, Chem. Eur. J. 20 (23) (2014) 6895–6908, https://doi.org/10.1002/chem.201304947.

[88] S.J. Sherlock, D.C. Boyd, B. Moasser, W.L. Gladfelter, Homogeneous catalytic carbonylation of nitroaromatics. 4. Preparation and characterization of ruthenium radical cations, Inorg. Chem. 30 (19) (1991) 3626–3632, https://doi.org/10.1021/ic00019a011.

[89] D. Fink, N. Orth, M. Linseis, I. Ivanović-Burmazović, R.F. Winter, Structural versatility and supramolecular isomerism in redox-active tetra- and hexaruthenium macrocycles, Eur. J. Inorg. Chem. (29) (2020) 2816–2829, https://doi.org/10.1002/ejic.202000387.

[90] N. Rotthowe, M. Linseis, L. Vogelsang, N. Orth, I. Ivanović-Burmazović, R. F. Winter, A "Pretender" croconate-bridged macrocyclic tetraruthenium complex: sizable redox potential splittings despite electronically insulated divinylphenylene diruthenium entities, Molecules 26 (17) (2021) 5232, https://doi.org/10.3390/molecules26175232.

[91] A. Ohta, K. Hattori, Y. Kusumoto, T. Kawase, T. Kobayashi, H. Naito, C. Kitamura, Effects of alkoxy substitution on the optical properties of 9,10-anthraquinone and anthracene: 2,3,6,7-tetrapropoxy-substituted vs. 2,6-dipropoxy-substituted derivatives, Chem. Lett. 41 (7) (2012) 674–676, https://doi.org/10.1246/cl.2012.674.

[92] V. Mishra, A. Raghuvanshi, A.K. Saini, S.M. Mobin, Anthracene derived dinuclear gold(I) diacetylide complexes: synthesis, photophysical properties and supramolecular interactions, J. Organomet. Chem. 813 (2016) 103–109, https://doi.org/10.1016/j.jorganchem.2016.04.013.

[93] S. Marquis, A. Moissette, H. Vezin, C. Brémard, Long-lived radical cation-electron pairs generated by anthracene sorption in non Brønsted acidic zeolites, J. Phys. Chem. B 109 (9) (2005) 3723–3726, https://doi.org/10.1021/jp0504120.

[94] C. Lambert, S. Amthor, J. Schelter, From valence trapped to valence delocalized by bridge state modification in bis(triarylamine) radical cations: evaluation of coupling matrix elements in a three-level system, J. Phys. Chem. A 108 (31) (2004) 6474–6486, https://doi.org/10.1021/jp048449s.

[95] C. Lambert, C. Risko, V. Coropceanu, J. Schelter, S. Amthor, N.E. Gruhn, J. C. Durivage, J.-L. Brédas, Electronic coupling in tetraanisylarylenediamine mixed-valence systems: the interplay between bridge energy and geometric factors, J. Am. Chem. Soc. 127 (23) (2005) 8508–8516, https://doi.org/10.1021/ja0512172.

[96] A. Rockenbauer, T. Vidóczy, Electronic Absorption Spectra of Radical Ions, Elsevier, Amsterdam, 1988.
[97] H. Vezin, A. Moissette, C. Brémard, Temperature-dependent interconversion of an anthracene radical cation/electron moiety to an electron-hole pair in the pores of Al-ZSM-5 zeolites, Angew. Chem. Int. Ed. 42 (45) (2003) 5587–5591, https://doi.org/10.1002/anie.200352269.
[98] A.L. Mattioda, L. Rutter, J. Parkhill, M. Head-Gordon, T.J. Lee, L.J. Allamandola, Near-infrared spectroscopy of nitrogenated polycyclic aromatic hydrocarbon cations from 0.7 to 2.5 μm, Astrophys. J. 680 (2) (2008) 1243–1255, https://doi.org/10.1086/529484.